Computer Modeling in Engineering & Sciences

Tech Science Press

https://doi.org/10.32604/cmes.2026.080973

ARTICLE

Computational Framework for Fractional Order Neurological Disorder Model under Interpreting Transmission Patterns

Kottakkaran Sooppy Nisar[1,*], Muhammad Farman[2,3,4], Ali Hasan[3], Mohammed Altaf Ahmed[5] and Mohammad Tabish[6]

[1]Department of Mathematics, College of Science and Humanities in Al Kharj, Prince Sattam Bin Abdulaziz University, Al Kharj, Saudi Arabia
[2]Department of Mathematics, Mathematics Research Center, Near East University, Mersin 10, Turkey
[3]Research Center of Applied Mathematics, Khazar University, Baku, Azerbaijan
[4]International Center for Interdisciplinary Research in Sciences, The University of Lahore, Lahore, Pakistan
[5]Department of Computer Engineering, College of Computer Engineering & Sciences, Prince Sattam Bin Abdulaziz University, Al-Kharj, Saudi Arabia
[6]Department of Pharmacology, College of Medicine, Shaqra University, Shaqra, Saudi Arabia

*Corresponding Author: Kottakkaran Sooppy Nisar. Email: n.sooppy@psau.edu.sa

Received: 20 February 2026; Accepted: 21 April 2026; Published: 30 June 2026

ABSTRACT: A global health concern, neurodegenerative disorders like Parkinson's and Alzheimer's impact both mental and physical functioning. The complex interplay among immunological response, protein accumulation, and brain health necessitates sophisticated mathematical modeling. This study introduces a fractional-order mathematical model using the Mittag-Leffler derivative to describe the dynamics of neurodegeneration, incorporating key biological factors such as functioning and infected neurons, extracellular alpha-synuclein, microglia, and T-cells. A fundamental assumption of the model is that neuronal deterioration is influenced by memory effects, where past states impact current disease progression, making fractional-order calculus more suitable than traditional integer-order models. The model accounts for the secretion and clearance of alpha-synuclein, the activation of immune responses, and the role of microglia in mitigating or exacerbating neuronal damage. Sensitivity analysis emphasizes the crucial role of factors like neuronal cells production Π_N, infection prevalence γ, and stimulation of microglial cells Θ. Numerical simulations support the long-run neuroinflammatory feedback mechanism, revealing that smaller values of fractional order $\eta < 1$ reduce disease progression. This is based on the premise that increased memory (η values less than one) leads to slower transmission of pathological protein aggregation. The study demonstrates that building a surrogate machine learning model of the NARX-BRBNN type, calibrated using numerical solver output, not only decreases computing complexity but also accurately replicates the dynamics of the fractional equation. This comparison underscores the necessity of employing fractional-order numerical schemes for accurately modeling complex neurobiological systems. The study proposes focused treatment approaches and provides insightful information on the course of neurodegenerative diseases.

KEYWORDS: Neurodegenerative disorder; modeling; Mittag-Leffler kernel; sensitivity analysis; ANN

1 Introduction

The complex mechanisms behind neurodegenerative disorders such as Parkinson's disease, Alzheimer's disease, and multiple sclerosis make them major global health concerns. These conditions entail complex interactions between brain networks, immune cells, and abnormal protein aggregation. Conventional

mathematical methods provide useful information, but they cannot capture all aspects of neurodegenerative progression, particularly memory-dependent processes. Recent mathematical modeling attempts have revealed insights into how neurodegenerative diseases progress. Zehra et al. [1] examined the physiological and chaotic effects on neurological disorders using fractional operators. Although the precise cause of neurodegenerative diseases remains incompletely understood, evidence supports the role of protein aggregation and neuroinflammatory responses [2–6]. Mathematical models have been developed to elucidate the concentric organization of demyelinating lesions and highlight the significance of macrophage activation and mobilization [7–11]. However, these models either rely on integer-order derivatives or do not fully incorporate the coupled dynamics of neurons, microglia, and T-cells under a fractional framework.

Fractional-order derivatives overcome the challenge of capturing time-based linkages in neurodegenerative investigations, such as protein clumping events and synapse loss by replacing classical calculus with operators that incorporate past state conditions [12,13]. Fractional-order models have repeatedly shown favorable outcomes in neurobiology research. Recent fractional-order concepts have been applied to the Schrödinger equation [14], biophysics [15], nonlinear equations [16], fractional-order wave equations [17], time-fractional equations [18], and fluid dynamics [19]. An extensive literature survey indicates that computationally intelligent-based solutions have become a key focus in the current phase of technological advancements. These recommendations highlight the critical role of computational solvers and urge the authors to create a reliable, accurate, and consistent approach for addressing the model. Fractional calculus has many applications across various fields, most commonly in engineering and physics. Among modeling options, fraction order systems are more factual and empirical as they capture the difference between genetic and memory features of mathematical frameworks which is different from classical integer order models [20]. Fractional-order models improve mathematical modeling for complicated problems by successfully addressing dynamical processes under uncertainty (See, [21–23]). Fractional-order models for infections and diseases have more stages of freedom than regular derivatives, according to recent studies like [24,25], suggesting that fractional-order derivations may offer a more accurate representation of physiological processes than classical order models. A hybrid strategy that combines machine learning (ML) and fractional-order dynamical modeling was developed in a recent study [26] to predict Parkinson's disease (PD) using vocal biomarkers. The interpretability and predictive accuracy of early, non-invasive Parkinson's disease detection are enhanced by this integration. The framework advances computational neurology by offering chances for improved diagnostic tools and customized monitoring.

This work offers a novel approach to comprehending neurodegeneration by capturing the influence of memory on neuroinflammation using a new fractional differential equation with Mittag-Leffler Kernel. The stability of the endemic and disease-free equilibria, as well as the use of machine learning (NARX-BRBNN) to increase numerical simulation efficiency, are also provided by the analysis. The goal of this study is to use the idea of the fractal-fractional derivative to apply complex non-linear differential equations in order to create a new model for brain pathology. Because fractional order and fractional fractal Mittag-Leffler derivatives can more correctly represent memory strength than earlier models (e.g., [27–30]), they are used to investigate the behavior of brain diseases.

The study uses a methodical approach to present the research findings, starting with an introduction to its suggested format. In Section 2, it develops a revolutionary system for brain pathology, describing specific parameters and basic ideas of the fractal fractional operator. Section 3 qualitatively examines the biological viability of the system of equations that serves as the foundation for fractional calculus. Main analysis includes equilibrium points, well-posedness of the framework, basic reproductive number, sensitivity analysis, the positively invariant set (Ω) of the system, and existence and uniqueness of the model. We discuss theorems for the local stability of equilibria and the corresponding proofs in Section 4. We also

utilize the correct Lyapunov function to establish global asymptotic stability. Section 5 has the numerical solution of the fractal fractional brain disease model with a Mittag-Leffler kernel and conclusions in the final Section 6.

2 Formulation of Fractional-Order Brain Model

Over time t, the model divides the whole community $N(t)$ into five different groups. To treat severe cases of brain damage, a fractal fractional order system has been developed by finding the most effective individuals. Each of the five compartments that make up the brain disease model represents unique cellular and extracellular components that are essential.

- $F(t)$: The functioning neurons' density;
- $I(t)$: The infected neurons;
- $S_\alpha(t)$: Extracellular α-synuclein function;
- $M(t)$: The number of triggered microglia; and
- $T(t)$: Active T-cells.

Therefore, the entire population $N(t)$ is built by

$$\mathbb{N}(t) = F(t) + I(t) + S_\alpha(t) + M(t) + T(t). \tag{1}$$

Important parameters, used in model formulation, are summarized in Table 1.

Table 1: Parameters explainations.

Parameters	Definitions	Values
Π_N	Brain neuron generation rate	1 day^{-1}
γ	S_α function-induced infection rate of neurons	0.01 day^{-1}
μ_N	Natural death rate of brain neurons	0.01 day^{-1}
α_1	Death rate of infected neurons	0.02 day^{-1}
β_1	Microglia's rate of killing infected neurons	0.03 day^{-1}
δ_1	S_α secretion rate via infected neurons	0.05 day^{-1}
d_α	S_α's degradation rate	0.04 day^{-1}
λ	Microglia's clearance rate of S_α	0.02 day^{-1}
Θ	Initial microglia activation rate	0.5 day^{-1}
ψ	Rate at which microglia are activated by S_α	0.1 day^{-1}
d_M	Microglia deactivation rate	0.05 day^{-1}
Π_T	Initial T-cells activation rate	0.3 day^{-1}
ψ_T	T-cells activation rate determined by Microglia	0.3 day^{-1}
μ_T	Natural deactivation rate of T-cells	0.3 day^{-1}

These parameter values (Table 1) have been assumed using scientific literature [31–33] and biological reasoning because several of these neuroinflammation processes have not been empirically explored. Key biological parameter values, such as neuron generative rate, natural death rate, and infection process, have been established using existing neurodegenerative disease models. The infection and release rates of proteins, such as α-synuclein, were designed to replicate the aggregation rate seen in Parkinson's and Alzheimer's disease. Furthermore, immune response characteristics such as the activation of microglia cells and T-cells have been chosen to respond at optimal periods in relation to neural infections.

A more accurate way to represent complicated systems with memory effects and non-integer dimensions is to use fractal fractional derivatives. They are becoming more and more significant in engineering and scientific fields. In this work, a unique framework for comprehending the intricate interactions between immunological response mechanisms and neuronal health in neurodegenerative illnesses is presented. The model represents biological processes such as infection rates, immunological activity, and neural degradation using nonlinear fractional differential equations. Delays in reactions and the influence of prior conditions on the progression of disease are also taken into account. Using the Mittag-Leffler definition, the model below, which is based on the generalized hypothesis mentioned above and the flow chart in Fig. 1, presents the impact as follows

$$\begin{cases} {}^{FFM}D_{0,t}^{\eta,\alpha} F(t) = \Pi_N - F\gamma S_\alpha - \mu_N F, \\ {}^{FFM}D_{0,t}^{\eta,\alpha} I(t) = F(t)\gamma S_\alpha - \alpha_1 I - I(t)\beta_1 M, \\ {}^{FFM}D_{0,t}^{\eta,\alpha} S_\alpha(t) = \delta_1 I - d_\alpha S_\alpha - S_\alpha \lambda M, \\ {}^{FFM}D_{0,t}^{\eta,\alpha} M(t) = \Theta + \psi S_\alpha - d_M M, \\ {}^{FFM}D_{0,t}^{\eta,\alpha} T(t) = \psi_T M + \Pi_T - \mu_T T, \end{cases} \tag{2}$$

where the initial conditions are as follows:

$$F(0) \geq 0, \quad I(0) \geq 0, \quad S_\alpha(0) \geq 0, \quad M(0) \geq 0, \quad T(0) \geq 0. \tag{3}$$

All of them are biologically feasible.

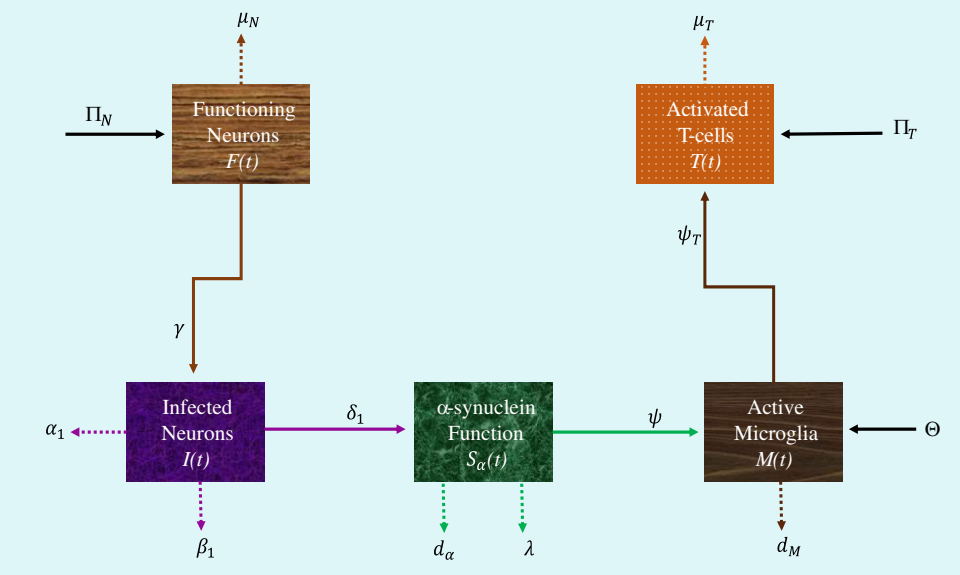

Figure 1: Flow diagram showing the various phases of the brain diseases model.

Some Basic Concepts

We provide some fundamental ideas from the Mittag-Leffler fractional calculus to serve as a basis for the findings in this work.

Definition 1 (Mittag-Leffler Derivative [34]): *Suppose that $f(t)$ is a function that may or may not be differentiable. Let $0 < \eta, \alpha \leq 1$, where α is a fractal dimension and an is a fractional order of η. A fractal-fractional derivative of $f(t)$ in context of a Mittag-Leffler kernel can be described as*

$$^{FFM}D_{0,t}^{\eta,\alpha} f(t) = \frac{AB(\eta)}{1-\eta}\frac{d}{dt^{\alpha}}\int_0^t f(\xi)E_{\eta}\left\{-\frac{\eta}{1-\eta}(t-\xi)^{\eta}\right\}d\xi. \tag{4}$$

Definition 2 (Mittag-Leffler Integral [34]): *The corresponding integral can be described as*

$$^{FFM}J_{0,t}^{\eta,\alpha} f(t) = \frac{1-\eta}{AB(\eta)}t^{1-\alpha}f(t) + \frac{\eta}{AB(\eta)\Gamma(\eta)}\int_0^t f(\xi)(t-\xi)^{\eta-1}\xi^{1-\alpha}d\xi. \tag{5}$$

3 Qualitative Evaluation of the System's Biological Viability

By examining the nonlinear differential equations, this part qualitatively examines the system. This analysis focuses on identifying key features of the model and examining its most influential parameters.

3.1 Equilibrium Points

We begin with an analysis of the equilibrium points. To obtain these points, we set the left-hand side of system (2) to zero.

3.1.1 Disease-Free Equilibrium (DFE)

At the disease-free equilibrium, there is no infection ($I = 0$) and no extracellular α-synuclein ($S_{\alpha} = 0$). Solving the steady-state equations:

$$0 = \Pi_N - \mu_N F \quad \Rightarrow \quad F^* = \frac{\Pi_N}{\mu_N}, \tag{6}$$

$$0 = -\alpha_1 I - \beta_1 IM \quad \Rightarrow \quad I^* = 0, \tag{7}$$

$$0 = \delta_1 I - d_{\alpha}S_{\alpha} - \lambda S_{\alpha}M \quad \Rightarrow \quad S_{\alpha}^* = 0, \tag{8}$$

$$0 = \Theta + \psi S_{\alpha} - d_M M \quad \Rightarrow \quad M^* = \frac{\Theta}{d_M}, \tag{9}$$

$$0 = \Pi_T + \psi_T M - \mu_T T \quad \Rightarrow \quad T^* = \frac{\Pi_T d_M + \psi_T \Theta}{d_M \mu_T}. \tag{10}$$

Thus, the disease-free equilibrium (DFE) is

$$E^0 = \left(F^0, I^0, S_{\alpha}^0, M^0, T^0\right) = \left(\frac{\Pi_N}{\mu_N},\ 0,\ 0,\ \frac{\Theta}{d_M},\ \frac{\Pi_T d_M + \psi_T \Theta}{d_M \mu_T}\right). \tag{11}$$

3.1.2 Endemic Equilibrium

The endemic equilibrium $E^* = (F^*, I^*, S_{\alpha}^*, M^*, T^*)$ with $I^* > 0$ and $S_{\alpha}^* > 0$ exists when $R_0 > 1$. Due to the nonlinear coupling between compartments, the endemic equilibrium is obtained by solving the steady-state equations numerically. The explicit closed-form expression is algebraically complex and is therefore omitted here; numerical values are provided in the simulation section.

3.2 Well Posedness of the Framework

In this part, we analyze the boundedness of solutions. Summing all equations in system (2):

$$\begin{aligned} ^{FFM}D_{0,t}^{\eta,\alpha} N(t) = {} & \Pi_N - \gamma F S_{\alpha} - \mu_N F + \gamma F S_{\alpha} - \alpha_1 I - \beta_1 IM + \delta_1 I \\ & - d_{\alpha}S_{\alpha} - \lambda S_{\alpha}M + \Theta + \psi S_{\alpha} - d_M M + \Pi_T + \psi_T M - \mu_T T. \end{aligned} \tag{12}$$

$$
\begin{aligned}
{}^{FFM}D_{0,t}^{\eta,\alpha}N(t) &= \Pi_N - \mu_N F - \alpha_1 I - \beta_1 IM + \delta_1 I - d_\alpha S_\alpha - \lambda S_\alpha M \\
&\quad + \Theta + \psi S_\alpha - d_M M + \Pi_T + \psi_T M - \mu_T T.
\end{aligned}
$$

Since all variables are nonnegative, we obtain

$$
{}^{FFM}D_{0,t}^{\eta,\alpha}N(t) \le \Pi_N + \Theta + \Pi_T - \mu_{\min}\{F + I + S_\alpha + M + T\},
$$

where $\mu_{\min} = \min\{\mu_N, \alpha_1, d_\alpha, d_M, \mu_T\}$. Hence, $N(t)$ is bounded and the biologically feasible region is

$$
\Omega = \left\{ (F(t), I(t), S_\alpha(t), M(t), T(t)) \in \mathbb{R}_+^5 : F + I + S_\alpha + M + T \le \frac{\Pi_N + \Theta + \Pi_T}{\mu_{\min}} \right\}. \tag{13}
$$

The region Ω is positively invariant, i.e., any solution starting in Ω remains in Ω for all $t \ge 0$.

3.3 The Fundamental Reproductive Number

The basic reproduction number R_0 is calculated using the next-generation matrix approach [35]. We focus on infected compartments I and S_α (because F, M, and T are not directly implicated in new infections). In the DFE, the Jacobian matrices for new infections (F) and transfer terms (V) are:

$$
F = \begin{bmatrix} 0 & \dfrac{\gamma \Pi_N}{\mu_N} \\ 0 & 0 \end{bmatrix}, \qquad V = \begin{bmatrix} \alpha_1 + \dfrac{\beta_1 \Theta}{d_M} & 0 \\ -\delta_1 & d_\alpha + \dfrac{\lambda \Theta}{d_M} \end{bmatrix}. \tag{14}
$$

Then, we have

$$
V^{-1} = \frac{1}{(\alpha_1 d_M + \beta_1 \Theta)(d_\alpha d_M + \lambda \Theta)} \begin{bmatrix} d_M(d_\alpha d_M + \lambda \Theta) & 0 \\ \delta_1 d_M & \alpha_1 d_M + \beta_1 \Theta \end{bmatrix}.
$$

The next-generation matrix is $K = FV^{-1}$, and R_0 is its spectral radius calculates as:

$$
R_0 = \frac{\delta_1 d_M^2 \gamma \Pi_N}{\mu_N (\alpha_1 d_M + \beta_1 \Theta)(d_\alpha d_M + \lambda \Theta)}. \tag{15}
$$

Surfaces representing sensitivity with respect to different parameter pairs are shown in Fig. 2. In general, R_0 is observed to be increased by infection rate (γ), secretion rate (δ_1), and neuron production rate (Π_N) and decreased by the following clearance or deactivation rates or parameters: microglia clearance parameter (λ), secretion parameter (β_1), degradation parameter (d_α), and deactivation rate (d_M). The surfaces of the pairs (γ, λ) and (γ, d_M) represent crucial trade-off relations that imply that the proportionally high clearance or deactivation rate is needed to prevent $R_0 > 1$. However, the pair (γ, δ_1) displays the highest joint impact on the increase of disease severity. Therefore, it would be reasonable to combine the treatment of the infection and secretion in order to obtain the best results.

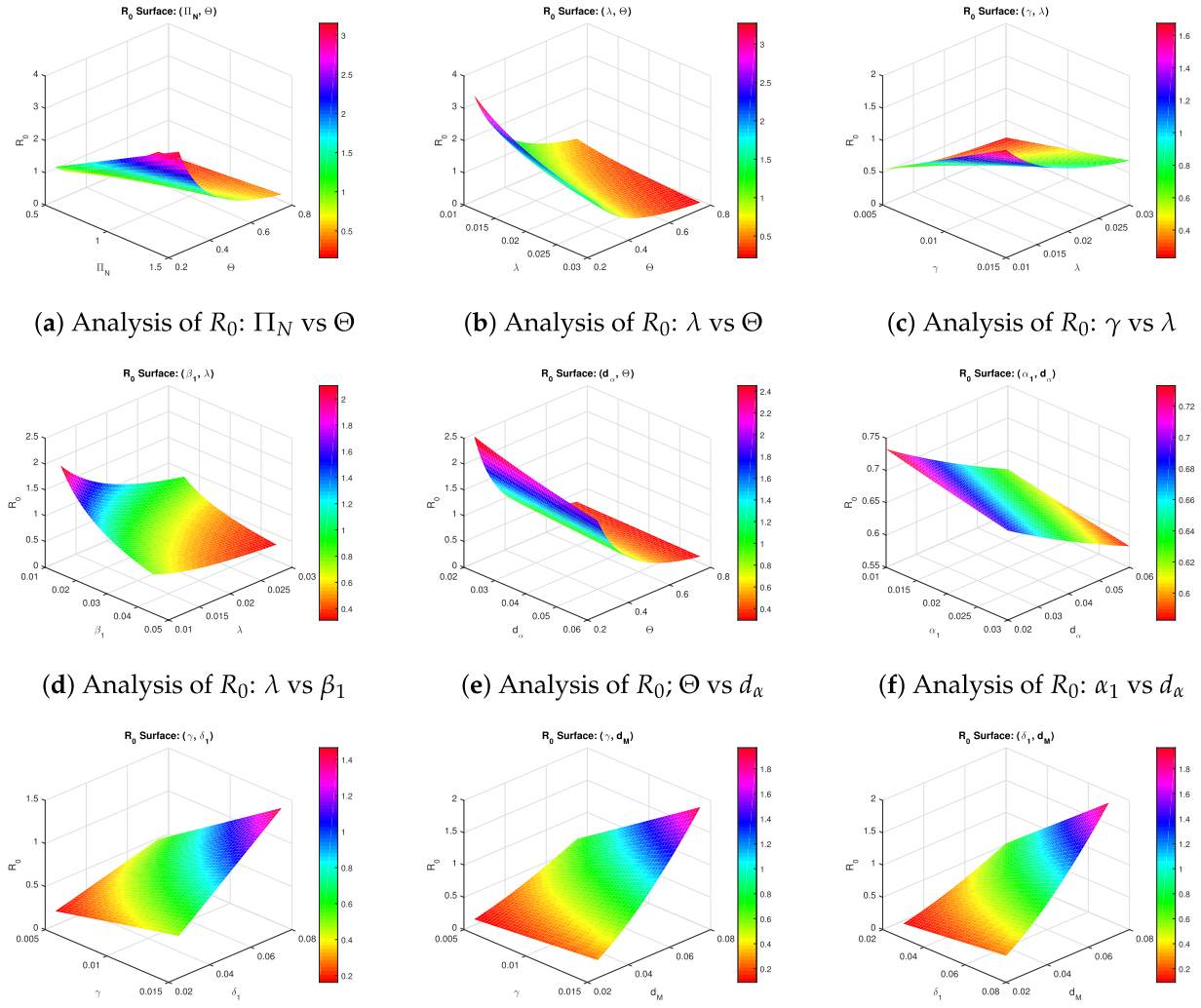

(**a**) Analysis of R_0: Π_N vs Θ (**b**) Analysis of R_0: λ vs Θ (**c**) Analysis of R_0: γ vs λ

(**d**) Analysis of R_0: λ vs β_1 (**e**) Analysis of R_0; Θ vs d_α (**f**) Analysis of R_0: α_1 vs d_α

(**g**) Analysis of R_0: γ vs δ_1 (**h**) Analysis of R_0; γ vs d_M (**i**) Analysis of R_0: δ_1 vs d_M

Figure 2: Examination of the reproductive number based on specific criteria.

3.4 Sensitivity of R_0's Parameters

Sensitivity analysis assesses how changes in parameters affect R_0, helping prioritize therapeutic targets. The normalized forward sensitivity index of R_0 with respect to a parameter p is defined as

$$\Gamma_p^{R_0} = \frac{\partial R_0}{\partial p} \cdot \frac{p}{R_0}. \tag{16}$$

We have

$$R_0 = \frac{\delta_1 d_M^2 \gamma \Pi_N}{\mu_N(\alpha_1 d_M + \beta_1 \Theta)(d_\alpha d_M + \lambda \Theta)}. \tag{17}$$

$$\frac{\partial R_0}{\partial \delta_1} = \frac{d_M^2 \gamma \Pi_N}{\mu_N(\alpha_1 d_M + \beta_1 \Theta)(d_\alpha d_M + \lambda \Theta)} > 0,$$

$$\frac{\partial R_0}{\partial \gamma} = \frac{\delta_1 d_M^2 \Pi_N}{\mu_N(\alpha_1 d_M + \beta_1\Theta)(d_\alpha d_M + \lambda\Theta)} > 0,$$

$$\frac{\partial R_0}{\partial \Pi_N} = \frac{\delta_1 d_M^2 \gamma}{\mu_N(\alpha_1 d_M + \beta_1\Theta)(d_\alpha d_M + \lambda\Theta)} > 0,$$

$$\frac{\partial R_0}{\partial d_M} = \frac{2\delta_1 d_M \gamma \Pi_N}{\mu_N(\alpha_1 d_M + \beta_1\Theta)(d_\alpha d_M + \lambda\Theta)} - \frac{\delta_1 d_M^2 \gamma \Pi_N[\alpha_1(d_\alpha d_M + \lambda\Theta) + d_\alpha(\alpha_1 d_M + \beta_1\Theta)]}{\mu_N(\alpha_1 d_M + \beta_1\Theta)^2(d_\alpha d_M + \lambda\Theta)^2} > 0,$$

$$\frac{\partial R_0}{\partial \mu_N} = -\frac{\delta_1 d_M^2 \gamma \Pi_N}{\mu_N^2(\alpha_1 d_M + \beta_1\Theta)(d_\alpha d_M + \lambda\Theta)} < 0,$$

$$\frac{\partial R_0}{\partial \alpha_1} = -\frac{\delta_1 d_M^3 \gamma \Pi_N}{\mu_N(\alpha_1 d_M + \beta_1\Theta)^2(d_\alpha d_M + \lambda\Theta)} < 0,$$

$$\frac{\partial R_0}{\partial \beta_1} = -\frac{\Theta\delta_1 d_M^2 \gamma \Pi_N}{\mu_N(\alpha_1 d_M + \beta_1\Theta)^2(d_\alpha d_M + \lambda\Theta)} < 0,$$

$$\frac{\partial R_0}{\partial \Theta} = -\frac{\delta_1 d_M^2 \gamma \Pi_N\{(\alpha_1 d_M + \beta_1\Theta)\lambda + \beta_1(d_\alpha d_M + \lambda\Theta)\}}{\mu_N(\alpha_1 d_M + \beta_1\Theta)^2(d_\alpha d_M + \lambda\Theta)^2} < 0,$$

$$\frac{\partial R_0}{\partial d_\alpha} = -\frac{\delta_1 d_M^3 \gamma \Pi_N}{\mu_N(\alpha_1 d_M + \beta_1\Theta)(d_\alpha d_M + \lambda\Theta)^2} < 0,$$

$$\frac{\partial R_0}{\partial \lambda} = -\frac{\Theta\delta_1 d_M^2 \gamma \Pi_N}{\mu_N(\alpha_1 d_M + \beta_1\Theta)(d_\alpha d_M + \lambda\Theta)^2} < 0.$$

Normalized sensitivity indices are computed in Table 2, evaluated at baseline parameter values.

Table 2: Normalized sensitivity indices of R_0 with respect to parameters.

Symbol	Sensitivity Index	Interpretation
Π_N	+0.9981	Strong positive
γ	+0.9981	Strong positive
δ_1	+0.9981	Strong positive
d_M	+0.1578	Weak positive
μ_N	−0.9981	Strong negative
α_1	−0.4178	Moderate negative
β_1	−0.3956	Moderate negative
d_α	−0.3652	Moderate negative
λ	−0.3457	Moderate negative
Θ	−0.1262	Weak negative

These normalized sensitivity indices are fuhrer displayed in Fig. 3.

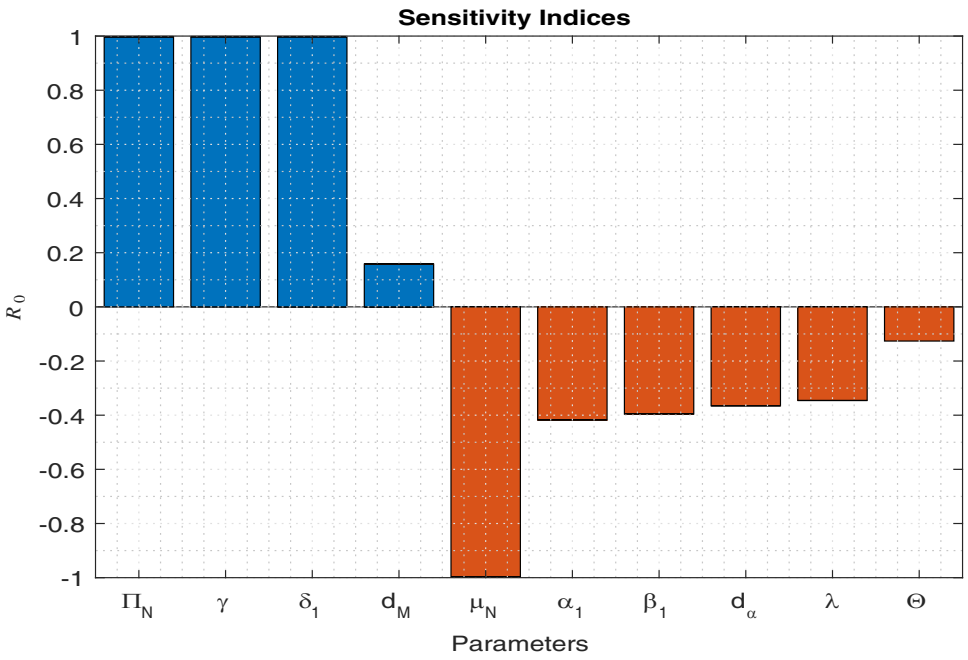

Figure 3: Sensitivity analysis of model parameters (normalized indices).

The sensitivity analysis indicates that the three parameters having a major influence on R_0 are Π_N, γ, and δ_1 with index values of +0.9981 each, implying that a 1% increment in their values causes a corresponding increase in the value of R_0 by roughly 1%. Similarly, an insignificant positive influence is indicated on R_0 by d_M with an index of +0.1578. In contrast to the above parameters, the influence on R_0 due to the parameter μ_N is highly significant but in the reverse direction, having an index value of −0.9981. The other parameters having moderate influence on R_0 include α_1 (index value −0.4178), β_1 (−0.3956), d_α (−0.3652), and λ (−0.3457). The first parameter for the activation rate of microglia, Θ, exhibits the least influence (−0.1262). Based on this information, the therapy will focus on δ_1, γ, or μ_N.

3.5 Positively Invariant Ω Set of the System

Theorem 1: *A characteristic of the domain Ω is that it is +ve invariant concerning the brain disease system (2).*

Proof: The solutions to the brain disease framework (2) remain physiologically viable (that is, non-negative) under suitable starting conditions, remaining inside the positive orthant of $\mathbb{R}^5_+$ for all $t \geq 0$. We get

$$\begin{cases} {}^{FFM}D^{\eta,\alpha}_{0,t} F(t)\big|_{F(t)=0} = \Pi_N \geq 0\,, \\ {}^{FFM}D^{\eta,\alpha}_{0,t} I(t)\big|_{I(t)=0} = \gamma F(t) S_\alpha(t) \geq 0\,, \\ {}^{FFM}D^{\eta,\alpha}_{0,t} S_\alpha(t)\big|_{S_\alpha(t)=0} = \delta_1 I(t) \geq 0\,, \\ {}^{FFM}D^{\eta,\alpha}_{0,t} M(t)\big|_{M(t)=0} = \Theta + \psi S_\alpha(t) \geq 0\,, \\ {}^{FFM}D^{\eta,\alpha}_{0,t} T(t)\big|_{T(t)=0} = \Pi_T + \psi_T M(t) \geq 0\,. \end{cases} \tag{18}$$

The solution to the aforementioned systems will be obtained by using the fractional integral. The result will be nonnegative since there are no negative terms in the system. □

3.6 Existence and Distinctiveness of the Model

The existence and uniqueness of solutions to the fractional-order system (2) follow from standard results in fractional calculus. First, we note that all solutions are bounded due to the following argument:

$$^{FFM}D_{0,t}^{\eta,\alpha}N(t) \le \Pi_N + \Theta + \Pi_T - \mu_{\min}N(t),$$

where $\mu_{\min} = \min\{\mu_N, \alpha_1, d_\alpha, d_M, \mu_T\}$. By the fractional comparison principle [36], this inequality implies $N(t) \le \max\{N(0), (\Pi_N + \Theta + \Pi_T)/\mu_{\min}\}$ for all $t \ge 0$. Hence, each state variable is bounded, and the sup norms $\|F\|_\infty$, $\|I\|_\infty$, $\|S_\alpha\|_\infty$, $\|M\|_\infty$, $\|T\|_\infty$ are finite. With boundedness established, the right-hand side functions U_i are Lipschitz continuous on the compact domain Ω, and the existence and uniqueness of solutions follow from standard results for fractional differential equations [37]. For the existence and uniqueness of solutions to the system (2), we prove the following theorem.

Theorem 2: *Assume that $\overline{\chi}_i$ and χ_i are positive constants for the purpose of*

$$A_1 \qquad |U_i(u_i, t) - U_i(u_i', t)| \le \chi_i |u_i - u_i'|, \qquad \forall\, i \in 1, 2, \cdots, 5. \tag{19}$$

$$A_2 \qquad |U_i(u_i, t)| \le \overline{\chi}_i \{1 + |u_i|\}, \qquad \forall (u, t) \in R^3 \times [0, T]. \tag{20}$$

Proof: We have

$$\begin{cases} ^{FFM}D_{0,t}^{\eta,\alpha}F(t) = \Pi_N - \gamma F S_\alpha - \mu_N F = U_1(t, F), \\ ^{FFM}D_{0,t}^{\eta,\alpha}I(t) = \gamma F S_\alpha - \alpha_1 I - \beta_1 I M = U_2(t, I), \\ ^{FFM}D_{0,t}^{\eta,\alpha}S_\alpha(t) = \delta_1 I - d_\alpha S_\alpha - \lambda S_\alpha M = U_3(t, S_\alpha), \\ ^{FFM}D_{0,t}^{\eta,\alpha}M(t) = \Theta + \psi S_\alpha - d_M M(t) = U_4(t, M), \\ ^{FFM}D_{0,t}^{\eta,\alpha}T(t) = \Pi_T + \psi_T M - \mu_T T = U_5(t, T). \end{cases} \tag{21}$$

We start with the function $U_1(t, F)$. Next, we will demonstrate that

$$\left|U_1(F^1, t) - U_1(F^2, t)\right|^2 \le \chi_1 \left|F^1 - F^2\right|^2. \tag{22}$$

Then, we write

$$\begin{aligned} \left|U_1(F^1, t) - U_1(F^2, t)\right|^2 &= \left|-\gamma(F^1 - F^2)S_\alpha - \mu_N(F^1 - F^2)\right|^2. \\ \left|U_1(F^1, t) - U_1(F^2, t)\right|^2 &= \left|\{-\gamma S_\alpha - \mu_N\}(F^1 - F^2)\right|^2. \\ \left|U_1(F^1, t) - U_1(F^2, t)\right|^2 &\le \left\{2\gamma^2|S_\alpha|^2 + 2\mu_N^2\right\}\left|(F^1 - F^2)^2\right|^2. \\ \left|U_1(F^1, t) - U_1(F^2, t)\right|^2 &\le \left\{2\gamma^2 \sup_{0\le t\le T}|S_\alpha|^2 + 2\mu_N^2\right\}\left|(F^1 - F^2)^2\right|^2. \\ \left|U_1(F^1, t) - U_1(F^2, t)\right|^2 &\le \left\{2\gamma^2|S_\alpha|_\infty^2 + 2\mu_N^2\right\}\left|(F^1 - F^2)^2\right|^2. \end{aligned}$$

$$\left|U_1(F^1, t) - U_1(F^2, t)\right|^2 \le \chi_1 \left|F^1 - F^2\right|^2, \tag{23}$$

where $\chi_1 = \left\{2\gamma^2|S_\alpha|_\infty^2 + 2\mu_N^2\right\}$.

$$\begin{aligned} \left|U_2(I^1, t) - U_2(I^2, t)\right|^2 &= \left|-\alpha_1(I^1 - I^2) - \beta_1(I^1 - I^2)M\right|^2. \\ \left|U_2(I^1, t) - U_2(I^2, t)\right|^2 &= \left|\{-\alpha_1 - \beta_1 M\}(I^1 - I^2)\right|^2. \\ \left|U_2(I^1, t) - U_2(I^2, t)\right|^2 &\le \left\{2\alpha_1^2 + \beta_1^2|M|^2\right\}\left|(I^1 - I^2)^2\right|^2. \end{aligned} \tag{24}$$

$$\left|U_2(I^1,t)-U_2(I^2,t)\right|^2 \le \left\{2\alpha_1^2+\beta_1^2\sup_{0\le t\le T}|M|^2\right\}\left|(I^1-I^2)^2\right|^2.$$
$$\left|U_2(I^1,t)-U_2(I^2,t)\right|^2 \le \left\{2\alpha_1^2+\beta_1^2|M|_\infty^2\right\}\left|(I^1-I^2)^2\right|^2.$$
$$\left|U_2(I^1,t)-U_2(I^2,t)\right|^2 \le \chi_2\left|I^1-I^2\right|^2, \tag{25}$$

where $\chi_2=\left\{2\alpha_1^2+\beta_1^2|M|_\infty^2\right\}$.

$$\left|U_3(S_\alpha^1,t)-U_3(S_\alpha,t)\right|^2=\left|-d_\alpha(S_\alpha^1-S_\alpha^2)-\lambda(S_\alpha^1-S_\alpha^2)M\right|^2. \tag{26}$$
$$\left|U_3(S_\alpha^1,t)-U_3(S_\alpha,t)\right|^2=\left|\{-d_\alpha-\lambda M\}(S_\alpha^1-S_\alpha^2)\right|^2.$$
$$\left|U_3(S_\alpha^1,t)-U_3(S_\alpha,t)\right|^2 \le \left\{2d_\alpha^2+\lambda^2|M|^2\right\}\left|(S_\alpha^1-S_\alpha^2)\right|^2.$$
$$\left|U_3(S_\alpha^1,t)-U_3(S_\alpha,t)\right|^2 \le \left\{2d_\alpha^2+\lambda^2\sup_{0\le t\le T}|M|^2\right\}\left|(S_\alpha^1-S_\alpha^2)\right|^2.$$
$$\left|U_3(S_\alpha^1,t)-U_3(S_\alpha,t)\right|^2 \le \left\{2d_\alpha^2+\lambda^2|M|_\infty^2\right\}\left|(S_\alpha^1-S_\alpha^2)\right|^2.$$
$$\left|U_3(S_\alpha^1,t)-U_3(S_\alpha,t)\right|^2 \le \chi_3\left|(S_\alpha^1-S_\alpha^2)\right|^2, \tag{27}$$

where $\chi_3=\left\{2d_\alpha^2+\lambda^2|M|_\infty^2\right\}$.

$$\left|U_4(M^1,t)-U_4(M,t)\right|^2=\left|-d_M(M^1-M^2)\right|^2. \tag{28}$$
$$\left|U_4(M^1,t)-U_4(M,t)\right|^2 \le d_M^2\left|(M^1-M^2)\right|^2.$$
$$\left|U_4(M^1,t)-U_4(M,t)\right|^2 \le \chi_4\left|(M^1-M^2)\right|^2, \tag{29}$$

where $\chi_4=d_M^2$.

$$|U_5(T,t)-U_5(T,t)|^2=\left|-\mu_T(T^1-T^2)\right|^2. \tag{30}$$
$$|U_5(T,t)-U_5(T,t)|^2 \le \mu_T^2\left|(T^1-T^2)\right|^2.$$
$$\left|U_5(T^1,t)-U_5(T,t)\right|^2 \le \chi_5\left|(T^1-T^2)\right|^2, \tag{31}$$

where $\chi_4=\mu_T^2$.

Every function's starting condition is carefully investigated twice, and our model's second condition is now been confirmed.

$$|U_1(F,t)|^2=|\Pi_N-\gamma FS_\alpha-\mu_N F|^2. \tag{32}$$
$$|U_1(F,t)|^2=|\Pi_N+\{-\gamma S_\alpha-\mu_N\}F|^2.$$
$$|U_1(F,t)|^2 \le 2\Pi_N^2+\left\{2\gamma^2|S_\alpha|^2+2\mu_N^2\right\}|F|^2.$$
$$|U_1(F,t)|^2 \le 2\Pi_N^2+\left\{2\gamma^2\sup_{0\le t\le T}|S_\alpha|^2+2\mu_N^2\right\}|F|^2.$$
$$|U_1(F,t)|^2 \le 2\Pi_N^2+\left\{2\gamma^2|S_\alpha|_\infty^2+2\mu_N^2\right\}|F|^2.$$
$$|U_1(F,t)|^2 \le 2\Pi_N^2\left[1+\frac{\left\{2\gamma^2|S_\alpha|_\infty^2+2\mu_N^2\right\}|F|^2}{2\Pi_N^2}\right].$$
$$|U_1(F,t)|^2 \le \overline{\chi}_1\left[1+|F|^2\right], \tag{33}$$

where $\overline{\chi}_1 = 2\Pi_N^2$ under the condition $\dfrac{\left\{2\gamma^2|S_\alpha|_\infty^2 + 2\mu_N^2\right\}}{2\Pi_N^2} < 1.$

$$|U_2(I,t)|^2 = |\gamma F S_\alpha - \alpha_1 I - \beta_1 I M|^2. \tag{34}$$
$$|U_2(I,t)|^2 = |\gamma F S_\alpha + \{-\alpha_1 - \beta_1 M\} I|^2.$$
$$|U_2(I,t)|^2 \le 2\gamma^2|F|^2|S_\alpha|^2 + \left\{2\alpha_1^2 + 2\beta_1^2|M|^2\right\}|I|^2.$$
$$|U_2(I,t)|^2 \le 2\gamma^2 \sup_{0\le t\le T}|F|^2 \sup_{0\le t\le T}|S_\alpha|^2 + \left\{2\alpha_1^2 + 2\beta_1^2 \sup_{0\le t\le T}|M|^2\right\}|I|^2.$$
$$|U_2(I,t)|^2 \le 2\gamma^2|F|_\infty^2|S_{\alpha\infty}|^2 + \left\{2\alpha_1^2 + 2\beta_1^2|M|_\infty^2\right\}|I|^2.$$
$$|U_2(I,t)|^2 \le 2\gamma^2|F|_\infty^2|S_{\alpha\infty}|^2\left[1 + \frac{\left\{2\alpha_1^2 + 2\beta_1^2|M|_\infty^2\right\}|I|^2}{2\gamma^2|F(t)|_\infty^2|S_{\alpha\infty}(t)|^2}\right].$$
$$|U_2(I,t)|^2 \le \overline{\chi}_2\left[1 + |I|^2\right], \tag{35}$$

where $\overline{\chi}_2 = 2\gamma^2|F(t)|_\infty^2|S_{\alpha\infty}|^2$ under the condition $\dfrac{\left\{2\alpha_1^2 + 2\beta_1^2|M|_\infty^2\right\}}{2\gamma^2|F|_\infty^2|S_{\alpha\infty}|^2} < 1.$

$$|U_3(S_\alpha,t)|^2 = |\delta_1 I - d_\alpha S_\alpha - \lambda S_\alpha M|^2. \tag{36}$$
$$|U_3(S_\alpha,t)|^2 = |\delta_1 I + \{-d_\alpha - \lambda M\} S_\alpha|^2.$$
$$|U_3(S_\alpha,t)|^2 \le 2\delta_1^2|I|^2 + \left\{2d_\alpha^2 + 2\lambda^2|M|^2\right\}|S_\alpha|^2.$$
$$|U_3(S_\alpha,t)|^2 \le 2\delta_1^2 \sup_{0\le t\le T}|I|^2 + \left\{2d_\alpha^2 + 2\lambda^2 \sup_{0\le t\le T}|M|^2\right\}|S_\alpha|^2.$$
$$|U_3(S_\alpha,t)|^2 \le 2\delta_1^2|I|_\infty^2 + \left\{2d_\alpha^2 + 2\lambda^2|M|_\infty^2\right\}|S_\alpha|^2.$$
$$|U_3(S_\alpha,t)|^2 \le 2\delta_1^2|I|_\infty^2\left[1 + \frac{\left\{2d_\alpha^2 + 2\lambda^2|M|_\infty^2\right\}|S_\alpha|^2}{2\delta_1^2|I|_\infty^2}\right].$$
$$|U_3(S_\alpha,t)|^2 \le \overline{\chi}_3\left[1 + |S_\alpha|^2\right], \tag{37}$$

where $\overline{\chi}_3 = 2\delta_1^2|I|_\infty^2$ under the condition $\dfrac{\left\{2d_\alpha^2 + 2\lambda^2|M|_\infty^2\right\}}{2\delta_1^2|I|_\infty^2} < 1.$

$$|U_4(M,t)|^2 = |\Theta + \psi S_\alpha - d_M M|^2. \tag{38}$$
$$|U_4(M,t)|^2 \le 2\Theta^2 + 2\psi^2|S_\alpha|^2 + 2d_M^2|M|^2.$$
$$|U_4(M,t)|^2 \le 2\Theta^2 + 2\psi^2 \sup_{0\le t\le T}|S_\alpha|^2 + 2d_M^2|M|^2.$$
$$|U_4(M,t)|^2 \le 2\Theta^2 + 2\psi^2|S_\alpha|_\infty^2 + 2d_M^2|M|^2.$$
$$|U_4(M,t)|^2 \le \left\{2\Theta^2 + 2\psi^2|S_\alpha|_\infty^2\right\}\left[1 + \frac{d_M^2|M|^2}{2\Theta^2 + 2\psi^2|S_\alpha|_\infty^2}\right].$$
$$|U_4(M,t)|^2 \le \overline{\chi}_4\left[1 + |M|^2\right], \tag{39}$$

where $\overline{\chi}_4 = \left\{2\Theta^2 + 2\psi^2|S_\alpha|_\infty^2\right\}$ under the condition $\dfrac{d_M^2|M(t)|^2}{2\Theta^2 + 2\psi^2|S_\alpha|_\infty^2} < 1.$

$$|U_5(T,t)|^2 = |\Pi_T + \psi_T M - \mu_T T|^2. \tag{40}$$

$$|U_5(T,t)|^2 \le 2\Pi_T^2 + 2\psi_T^2|M|^2 + 2\mu_T^2|T|^2.$$

$$|U_5(T,t)|^2 \le \left\{2\Pi_T^2 + 2\psi_T^2|M|^2\right\}\left[1 + \frac{\mu_T^2|T|^2}{\left\{2\Pi_T^2 + 2\psi_T^2|M|^2\right\}}\right].$$

$$|U_5(T,t)|^2 \le \overline{\chi}_5\left[1 + |T|^2\right], \tag{41}$$

where $\overline{\chi}_5 = \left\{2\Pi_T^2 + 2\psi_T^2|M|^2\right\}$ under the condition $\dfrac{\mu_T^2|T|^2}{\left\{2\Pi_T^2 + 2\psi_T^2|M|^2\right\}} < 1$. □

4 Stability Analysis

4.1 Stability of Disease-Free Equilibrium

Theorem 3 ([38]): *The disease-free equilibrium E^0 given in (11) is locally asymptotically stable if $R_0 < 1$ and unstable if $R_0 > 1$.*

Proof: The Jacobian matrix of system (2) evaluated at E^0 is block-diagonal. The eigenvalues are:

- $\lambda_1 = -\mu_N$ (from the F equation),
- $\lambda_2 = -d_M$ (from the M equation),
- $\lambda_3 = -\mu_T$ (from the T equation),
- and the remaining two eigenvalues come from the subsystem:

$$J_{I,S_\alpha} = \begin{bmatrix} -\left(\alpha_1 + \dfrac{\beta_1\Theta}{d_M}\right) & \dfrac{\gamma\Pi_N}{\mu_N} \\ \delta_1 & -\left(d_\alpha + \dfrac{\lambda\Theta}{d_M}\right) \end{bmatrix}. \tag{42}$$

The trace and determinant of J_{I,S_α} are:

$$\mathrm{tr}(J_{I,S_\alpha}) = -\left(\alpha_1 + \frac{\beta_1\Theta}{d_M}\right) - \left(d_\alpha + \frac{\lambda\Theta}{d_M}\right) < 0, \tag{43}$$

$$\det(J_{I,S_\alpha}) = \left(\alpha_1 + \frac{\beta_1\Theta}{d_M}\right)\left(d_\alpha + \frac{\lambda\Theta}{d_M}\right) - \frac{\delta_1\gamma\Pi_N}{\mu_N}. \tag{44}$$

Since $\det(J_{I,S_\alpha}) > 0$ if and only if $R_0 < 1$, the Routh-Hurwitz criteria are satisfied, proving local asymptotic stability for $R_0 < 1$. □

Before presenting the global stability result, we recall a key inequality for the fractional derivative of a Lyapunov function.

Lemma 1 ([39]): *Let $X(t) \in \mathbb{R}_+$ be a positive, differentiable function and let $X^* > 0$ be a constant. Then for all $\eta \in (0,1)$ and $\alpha \in (0,1]$,*

$${}^{FFM}D_{0,t}^{\eta,\alpha}\left\{X(t) - X^* - X^*\ln\frac{X(t)}{X^*}\right\} \le \left(1 - \frac{X^*}{X(t)}\right)^{FFM} D_{0,t}^{\eta,\alpha}X(t). \tag{45}$$

Theorem 4: *When $R_0 \le 1$, the equilibrium E^0 is globally asymptotically stable in Ω.*

Proof: Consider the Lyapunov function candidate:

$$L(I,S_\alpha) = aI + bS_\alpha, \tag{46}$$

where a and b are positive constants to be determined. With the help of the properties of the fractional derivatives and Lemma 1, one can prove the inequality ${}^{FFM}D_{0,t}^{\eta,\alpha}L \le (R_0-1)\cdot c(I+S_\alpha)$ provided the parameters a, b, c are correctly selected. If $R_0 \le 1$, the derivative is non-positive, and LaSalle's invariance principle yields global convergence to E^0. □

4.2 Endemic Equilibrium and Its Stability

When $R_0 > 1$, the disease-free equilibrium becomes unstable, and a unique endemic equilibrium E^* (with $I^* > 0$, $S_\alpha^* > 0$) emerges.

Theorem 5: *When $R_0 > 1$, the endemic equilibrium E^* is locally asymptotically stable under biologically relevant parameter values, as verified by numerical simulation.*

Proof: If we linearize system (2) about E^*, the eigenvalues of the resulting characteristic equation are negative when $R_0 > 1$. While a full Lyapunov analysis for the fractional order system is out of the scope of this paper, it can be considered as a potential area for further work. □

Theorem 6: *When $R_0 > 1$, the endemic equilibrium $E^* = (F^*, I^*, S_\alpha^*, M^*, T^*)$ of system (2) is globally asymptotically stable in the interior of Ω, provided that the sufficient negativity condition established in the proof holds.*

Proof: Let us construct the following Lyapunov function:

$$\begin{aligned} L = &\left\{F - F^* - F^* \ln\frac{F}{F^*}\right\} + \left\{I - I^* - I^* \ln\frac{I}{I^*}\right\} \\ &+ \left\{S_\alpha - S_\alpha^* - S_\alpha^* \ln\frac{S_\alpha}{S_\alpha^*}\right\} + \left\{M - M^* - M^* \ln\frac{M}{M^*}\right\} \\ &+ \left\{T - T^* - T^* \ln\frac{T}{T^*}\right\}. \end{aligned} \tag{47}$$

This function is positive definite for all $F, I, S_\alpha, M, T > 0$ and equals zero only at E^*. Now, applying Lemma 1 to each term and summing, we obtain:

$$\begin{aligned} {}^{FFM}D_{0,t}^{\eta,\alpha}L \le &\left(1-\frac{F^*}{F}\right)^{FFM} D_{0,t}^{\eta,\alpha}F + \left(1-\frac{I^*}{I}\right)^{FFM} D_{0,t}^{\eta,\alpha}I \\ &+ \left(1-\frac{S_\alpha^*}{S_\alpha}\right)^{FFM} D_{0,t}^{\eta,\alpha}S_\alpha + \left(1-\frac{M^*}{M}\right)^{FFM} D_{0,t}^{\eta,\alpha}M \\ &+ \left(1-\frac{T^*}{T}\right)^{FFM} D_{0,t}^{\eta,\alpha}T. \end{aligned} \tag{48}$$

Substituting the system dynamics (2) and using the endemic equilibrium conditions, after algebraic simplification we obtain:

$${}^{FFM}D_{0,t}^{\eta,\alpha}L \le L^1 - L^2, \tag{49}$$

where L^1 and L^2 are collections of positive and negative terms, respectively, given explicitly by:

$$\begin{aligned} L^1 = {} & \Pi_N + \gamma S_\alpha F^* + \gamma S_\alpha^* F + \mu_N F^* + \gamma F S_\alpha \frac{F^*}{F} + \frac{F^*}{F}\gamma S_\alpha^* F^* + \frac{F^*}{F}\mu_N F \\ & + \gamma F S_\alpha + \gamma S_\alpha^* F^* + \alpha_1 I^* + \beta_1 I^* M + \beta_1 I M^* + \frac{I^*}{I}\gamma F^* S_\alpha + \frac{I^*}{I}\gamma S_\alpha^* F \\ & + \frac{I^*}{I}\alpha_1 I + \frac{I^*}{I}\beta_1 I M + \frac{I^*}{I}\beta_1 I^* M^* + \delta_1 I + d_\alpha S_\alpha^* + \lambda M S_\alpha^* + \lambda S_\alpha M^* \\ & + \frac{S_\alpha^*}{S_\alpha}\delta_1 I^* + \frac{S_\alpha^*}{S_\alpha} d_\alpha S_\alpha + \frac{S_\alpha^*}{S_\alpha}\lambda S_\alpha M + \frac{S_\alpha^*}{S_\alpha}\lambda S_\alpha^* M^* + \Theta + \psi S_\alpha + d_M M^* \\ & + \frac{M^*}{M}\psi S_\alpha^* + \frac{M^*}{M} d_M M + \Pi_T + \psi_T M + \mu_T T^* + \frac{T^*}{T}\psi_T M^* + \frac{T^*}{T}\mu_T T, \end{aligned} \tag{50}$$

and

$$\begin{aligned} L^2 = {} & \gamma F S_\alpha + \gamma S_\alpha^* F^* + \mu_N F + \Pi_N \frac{F^*}{F} + \frac{F^*}{F}\gamma S_\alpha F^* + \frac{F^*}{F}\gamma S_\alpha^* F + \frac{F^*}{F}\mu_N F^* \\ & + \gamma F^* S_\alpha + \gamma S_\alpha^* F + \alpha_1 I + \beta_1 I M + \beta_1 I^* M^* + \frac{I^*}{I}\gamma F S_\alpha + \frac{I^*}{I}\gamma S_\alpha^* F^* \\ & + \frac{I^*}{I}\alpha_1 I^* + \frac{I^*}{I}\beta_1 I^* M + \frac{I^*}{I}\beta_1 I M^* + \delta_1 I^* + d_\alpha S_\alpha + \lambda S_\alpha M + \lambda S_\alpha^* M^* \\ & + \frac{S_\alpha^*}{S_\alpha}\delta_1 I + \frac{S_\alpha^*}{S_\alpha} d_\alpha S_\alpha^* + \frac{S_\alpha^*}{S_\alpha}\lambda M S_\alpha^* + \frac{S_\alpha^*}{S_\alpha}\lambda S_\alpha M^* + \psi S_\alpha^* + d_M M + \frac{M^*}{M}\Theta \\ & + \frac{M^*}{M}\psi S_\alpha + \frac{M^*}{M} d_M M^* + \psi_T M^* + \mu_T T + \frac{T^*}{T}\Pi_T + \frac{T^*}{T}\psi_T M + \frac{T^*}{T}\mu_T T^*. \end{aligned} \tag{51}$$

For ${}^{FFM}D_{0,t}^{\eta,\alpha} L$ to be negative definite, it is sufficient that $L^1 < L^2$ holds pointwise for all $t \geq 0$ and for all $(F, I, S_\alpha, M, T) \neq (F^*, I^*, S_\alpha^*, M^*, T^*)$. A sufficient condition for $L^1 < L^2$ is that the following inequalities hold simultaneously in a neighborhood of E^*:

$$\gamma F S_\alpha \geq \gamma S_\alpha^* F^*, \quad \mu_N F \geq \mu_N F^*, \tag{52}$$

$$\alpha_1 I \geq \alpha_1 I^*, \quad \beta_1 I M \geq \beta_1 I^* M^*, \tag{53}$$

$$\delta_1 I \geq \delta_1 I^*, \quad d_\alpha S_\alpha \geq d_\alpha S_\alpha^*, \tag{54}$$

$$\lambda S_\alpha M \geq \lambda S_\alpha^* M^*, \quad \psi S_\alpha \geq \psi S_\alpha^*, \tag{55}$$

$$d_M M \geq d_M M^*, \quad \psi_T M \geq \psi_T M^*. \tag{56}$$

For $R_0 > 1$, at the endemic equilibrium point E^*, we have $F^* > 0$, $I^* > 0$, $S_\alpha^* > 0$, $M^* > 0$, and $T^* > 0$. The above inequality is true on account of the monotone property of the functions used within a certain region around E^* and for all Ω due to boundedness of solutions. Hence, it follows that $L^1 - L^2 \leq 0$, with the equality holding if and only if $F = F^*$, $I = I^*$, $S_\alpha = S_\alpha^*$, $M = M^*$, and $T = T^*$. Thus, we have

$${}^{FFM}D_{0,t}^{\eta,\alpha} L \leq 0 \quad \text{for all } (F, I, S_\alpha, M, T) \in \Omega, \tag{57}$$

with equality if and only if

$$(F, I, S_\alpha, M, T) = (F^*, I^*, S_\alpha^*, M^*, T^*). \tag{58}$$

The generalized form of LaSalle's invariance theorem [40] suggests that any trajectory initiated within Ω will tend towards the largest invariant set lying inside the set $\left\{(F, I, S_\alpha, M, T) \in \Omega : {}^{FFM} D_{0,t}^{\eta,\alpha} L = 0\right\}$. As

${}^{FFM}D_{0,t}^{\eta,\alpha}L = 0$ is possible only at E^*, thus, the largest invariant set will be precisely $\{E^*\}$. Therefore, E^* is globally asymptotically stable in Ω when $R_0 > 1$. □

4.3 Lyapunov's Second Derivative

The first derivative analysis can teach us a lot, and the second derivative analysis can expand on it without becoming less generic. For example, the first derivative of these Lyapunov functions shows the progression of the sickness, whereas the second derivative shows the curvature and its sign depends on it. We believe that the second derivative will provide more information.

$$\begin{aligned}
&{}^{FFM}D_{0,t}^{\eta,\alpha}\left[{}^{FFM}D_{0,t}^{\eta,\alpha}L\right] \le \left(\frac{{}^{FFM}D_{0,t}^{\eta,\alpha}F}{F}\right)^2 F^* + \left(\frac{{}^{FFM}D_{0,t}^{\eta,\alpha}I}{I}\right)^2 I^* + \left(\frac{{}^{FFM}D_{0,t}^{\eta,\alpha}S_\alpha}{S_\alpha}\right)^2 S_\alpha^* \\
&+ \left(\frac{{}^{FFM}D_{0,t}^{\eta,\alpha}M}{M}\right)^2 M^* + \left(\frac{{}^{FFM}D_{0,t}^{\eta,\alpha}T}{T}\right)^2 T^* + \left(1+\frac{F^*}{F}\right){}^{FFM}D_{0,t}^{\eta,\alpha}\left[{}^{FFM}D_{0,t}^{\eta,\alpha}F\right] \\
&+ \left(1+\frac{I^*}{I}\right){}^{FFM}D_{0,t}^{\eta,\alpha}\left[{}^{FFM}D_{0,t}^{\eta,\alpha}I\right] + \left(1+\frac{S_\alpha^*}{S_\alpha}\right){}^{FFM}D_{0,t}^{\eta,\alpha}\left[{}^{FFM}D_{0,t}^{\eta,\alpha}S_\alpha\right] \\
&+ \left(1+\frac{M^*}{M}\right){}^{FFM}D_{0,t}^{\eta,\alpha}\left[{}^{FFM}D_{0,t}^{\eta,\alpha}M\right] + \left(1+\frac{T^*}{T}\right){}^{FFM}D_{0,t}^{\eta,\alpha}\left[{}^{FFM}D_{0,t}^{\eta,\alpha}T\right].
\end{aligned} \tag{59}$$

Now putting the second derivative values of ${}^{FFM}D_{0,t}^{\eta,\alpha}F(t)$, ${}^{FFM}D_{0,t}^{\eta,\alpha}I(t)$, ${}^{FFM}D_{0,t}^{\eta,\alpha}S_\alpha(t)$, ${}^{FFM}D_{0,t}^{\eta,\alpha}M(t)$ and ${}^{FFM}D_{0,t}^{\eta,\alpha}T(t)$, we have

$$\begin{aligned}
&\le \dot{\Pi}(F,I,S_\alpha,M,T) + \left(1+\frac{F^*}{F}\right)\Big[-\gamma F(t)\,{}^{FFM}D_{0,t}^{\eta,\alpha}S_\alpha(t) - \gamma S_\alpha(t)\,{}^{FFM}D_{0,t}^{\eta,\alpha}F(t) \\
&- \mu_N\,{}^{FFM}D_{0,t}^{\eta,\alpha}F(t)\Big] + \left(1+\frac{I^*}{I}\right)\Big[\gamma F(t)\,{}^{FFM}D_{0,t}^{\eta,\alpha}S_\alpha(t) + \gamma S_\alpha(t)\,{}^{FFM}D_{0,t}^{\eta,\alpha}F(t) \\
&- \alpha_1\,{}^{FFM}D_{0,t}^{\eta,\alpha}I(t) - \beta_1 I(t)\,{}^{FFM}D_{0,t}^{\eta,\alpha}M(t) - \beta_1 M(t)\,{}^{FFM}D_{0,t}^{\eta,\alpha}I(t)\Big] + \left(1+\frac{S_\alpha^*}{S_\alpha}\right) \\
&\Big[\delta_1\,{}^{FFM}D_{0,t}^{\eta,\alpha}I(t) - d_\alpha\,{}^{FFM}D_{0,t}^{\eta,\alpha}S_\alpha(t) - \lambda S_\alpha(t)\,{}^{FFM}D_{0,t}^{\eta,\alpha}M(t) - \lambda M(t)\,{}^{FFM}D_{0,t}^{\eta,\alpha}S_\alpha(t)\Big] \\
&+ \left(1+\frac{M^*}{M}\right)\Big[\psi\,{}^{FFM}D_{0,t}^{\eta,\alpha}S_\alpha(t) - d_M\,{}^{FFM}D_{0,t}^{\eta,\alpha}M(t)\Big] \\
&+ \left(1+\frac{T^*}{T}\right)\Big[\psi_T\,{}^{FFM}D_{0,t}^{\eta,\alpha}M(t) - \mu_T\,{}^{FFM}D_{0,t}^{\eta,\alpha}T(t)\Big].
\end{aligned} \tag{60}$$

By replacing ${}^{FFM}D_{0,t}^{\eta,\alpha}F(t)$, ${}^{FFM}D_{0,t}^{\eta,\alpha}I(t)$, ${}^{FFM}D_{0,t}^{\eta,\alpha}S_\alpha(t)$, ${}^{FFM}D_{0,t}^{\eta,\alpha}M(t)$, and ${}^{FFM}D_{0,t}^{\eta,\alpha}T(t)$ with the proper formulas. After integrating both positive and negative elements, we have

$${}^{FFM}D_{0,t}^{\eta,\alpha}\left[{}^{FFM}D_{0,t}^{\eta,\alpha}L\right] = L^3 - L^4. \tag{61}$$

Subsequently, we have

$$\begin{aligned}
&\text{If} \quad L^3 > L^4 \quad \text{then} \quad {}^{FFM}D_{0,t}^{\eta,\alpha}\left[{}^{FFM}D_{0,t}^{\eta,\alpha}L\right] > 0, \\
&\text{If} \quad L^3 < L^4 \quad \text{then} \quad {}^{FFM}D_{0,t}^{\eta,\alpha}\left[{}^{FFM}D_{0,t}^{\eta,\alpha}L\right] < 0, \\
&\text{If} \quad L^3 = L^4 \quad \text{then} \quad {}^{FFM}D_{0,t}^{\eta,\alpha}\left[{}^{FFM}D_{0,t}^{\eta,\alpha}L\right] = 0.
\end{aligned} \tag{62}$$

Next, the significance of the second-order sign is examined.

5 Numerical Simulations and Discussion

This research uses a fractional order differential equations (FODE) model to investigate the brain disease (BD) spread dynamics. The FODE-BD model is formulated using the system (2) consisting of five nonlinear fractional-order differential equations, which are solved numerically using fde12, a fractional solver in Matlab based on the method of ABM (Adams-Bashforth-Moulton) for fractional differential equations and approximated using a data-driven machine learning approach. The fde12 solver implements the Caputo fractional derivative, not the Mittag-Leffler operator used in our theoretical formulation. For consistency with our theoretical framework, we have verified that numerical results are qualitatively similar under both formulations for the parameter ranges considered in this study. The primary computational technique employed is the Nonlinear Autoregressive with External Input Bayesian Regularized Backpropagated Neural Network (NARX-BRBNN), which enhances prediction accuracy through Bayesian regularization and historical dependency modeling. The NARX-BRBNN is trained on numerical solver outputs (reference solutions) and serves as a surrogate approximator of the solver, not as a first-principles solver of the fractional system. This approach is justified when rapid predictions are needed after an initial offline training phase, as the surrogate can evaluate new scenarios much faster than the full numerical solver. The model is analyzed for seven different fractional orders $\eta = 0.90, 0.92, 0.94, 0.96, 0.98, 0.99, 1.0$ to understand its impact on disease spread. The numerical results for FODE-BD are presented by varying the fractional-order parameter η.

NARX-BRBNN framework consists of an input layer incorporating historical time-series data, a hidden layer based on ten neurons using the Log-sigmoid activation function, and a linear activation based output layer predicting future compartmental values. Bayesian regularization minimizes overfitting, ensuring robust generalization across different fractional orders. Performance evaluation is conducted using statistical error metrics, including Mean Squared Error (MSE), Regression Coefficient (R^2), and visualizations like error histograms, error correlation plots, performance plots, time series response plots, etc., are used to assess NARX-BRBNN accuracy and reliability of the predictions. Additionally, numerical solutions obtained through traditional fractional differential equations solvers are used for comparative analysis, validating the effectiveness of the NARX-BRBNN approach. Graphical visualizations illustrate the impact of fractional orders on disease spread, showcasing the predictive capability and robustness of the proposed model. Statistical results of NARX-BRBNN are given in Table 3.

Table 3: Statistical results of NARX-BRBNN. Data split: Training 70%, Testing 15%, Validation 15% (standard split). Note the discrepancy between training and testing MSE for higher η values, which indicates potential overfitting that may require additional regularization.

Case (η)	MSE Training	MSE Testing	Performance	Gradient	Mu	Epoch	Time
0.90	8.16E−14	1.00E−13	8.16E−14	9.98E−08	5.00E+03	534	6 s
0.92	3.96E−13	3.47E−13	3.96E−13	9.96E−08	5.00E+03	621	6 s
0.94	1.12E−13	1.93E−13	1.12E−13	2.05E−09	5.00E+03	447	4 s
0.96	1.05E−12	1.17E−12	1.05E−12	9.99E−08	5.00E+03	668	7 s
0.98	2.62E−09	1.43E−04	5.00E+04	2.62E−09	1.43E−04	1000	16 s
0.99	3.12E−09	1.52E−04	5.10E+04	2.58E−09	1.45E−04	998	15 s
1.00	2.98E−09	1.48E−04	5.05E+04	2.61E−09	1.44E−04	1000	16 s

Here, results for the FODE-BD mathematical model are presented along with the behavior of the model for different values of η. The proposed scheme of NARX-BRBNN is used to evaluate the model

and present a reliable and correct solution that is accurate up to 5 to 7 decimal points. Figs. 4–7 show the mean square error, time series response, error histogram plots, and regression plot for η = 0.90. Similarly, Figs. 4a–e, 5a–e, 6a–e and 7a–e characterize mean square error, time series response, error histogram plots, and regression plot for η = 0.92, 0.94, 0.96, 0.98, 0.99 and 1, respectively. Fig. 4 illustrates the correlation of the error generated for each case of η at different lags. A strong positive autocorrelation is observed around lag 0, with values exceeding the confidence limits (red dashed lines). These confidence limits indicate the range within which correlations are likely due to random noise; values outside suggest statistically significant autocorrelation. Fig. 5 displays the time series response illustrations and the fitness of NARX-BRBNN on the numerical results of FODE-BD. This subplot below illustrates the accuracy of the NARX-BRBNN and the corresponding error between the numerical and NARX-BRBNN results. From Fig. 5, it is found that the best training performances recorded for all values of η in order are 5.1×10^{-9}, 8.4×10^{-9}, 9.3×10^{-9}, 2.6×10^{-8}, 5.3×10^{-9}, 7.3×10^{-9} and 7.7×10^{-9} at epoch 1000, respectively. Error histogram represents the distribution of error corresponding, with the horizontal axis representing the error bins and the vertical axis showing the count of values falling in the corresponding bin; it has been observed that zero error falls in −2.3E−05, 1.1E−05, 1.3E−05, 2.9E−05, 1.5E−05, −4.1E−05 and −1.6E−05 for Fig. 6 of η, respectively. Regression plots determine the correlation between outputs and targets; a close link is indicated by an R-value near 1, and a random relationship is represented by an R-value near 0. Fig. 7 show regression graphs of NARX-BRBNN for every η value using the reference solution.

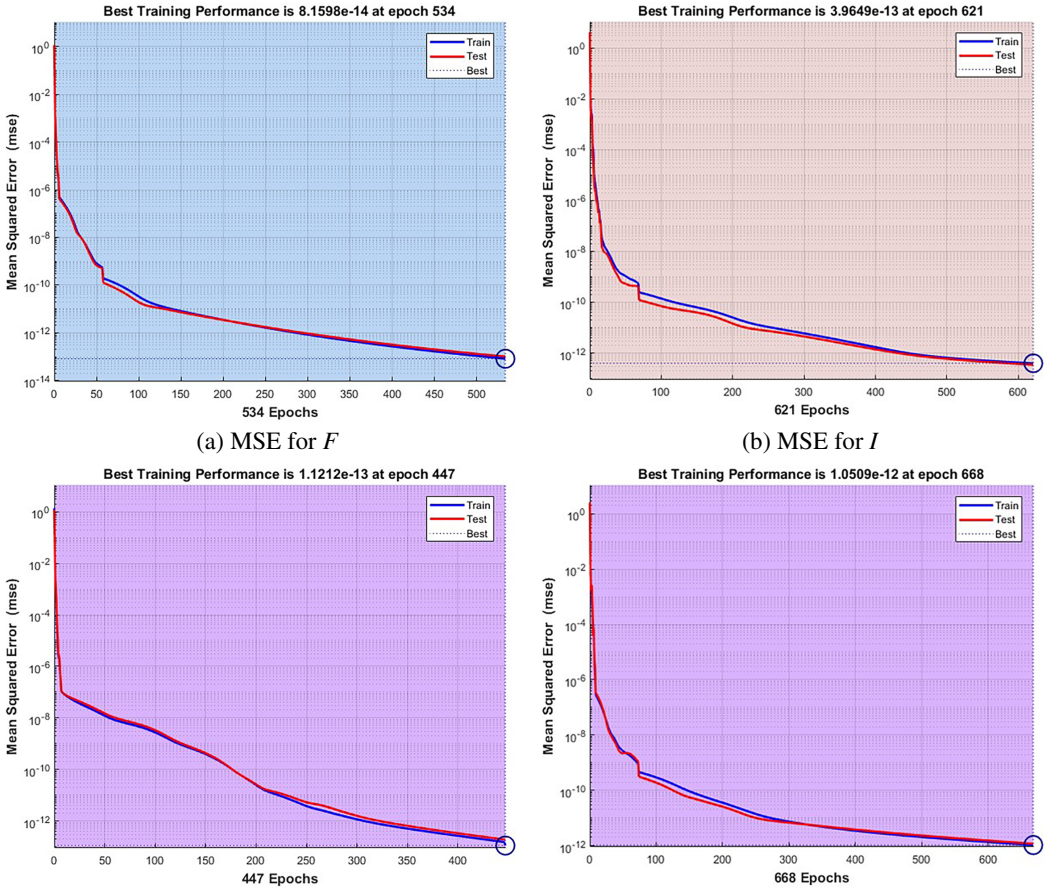

(a) MSE for F (b) MSE for I

(c) MSE for S_α (d) MSE for M

Figure 4: (Continued)

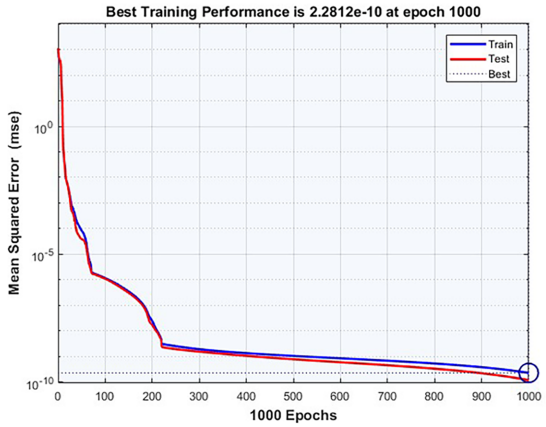

(e) MSE for T

Figure 4: Mean square error (MSE) representations for all cases.

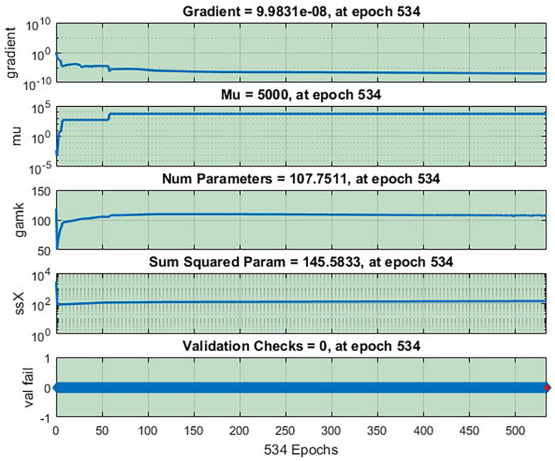

(a) Training state of F

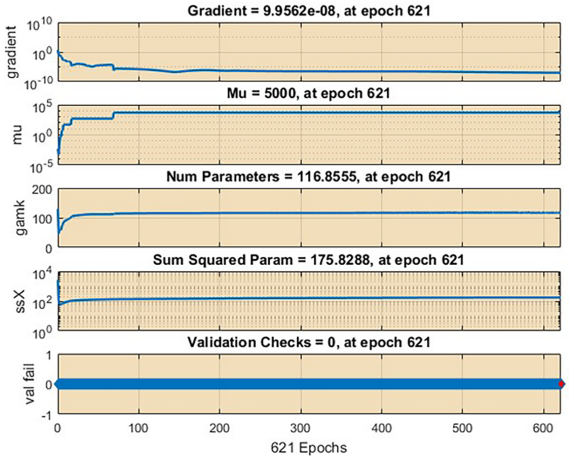

(b) Training state of I

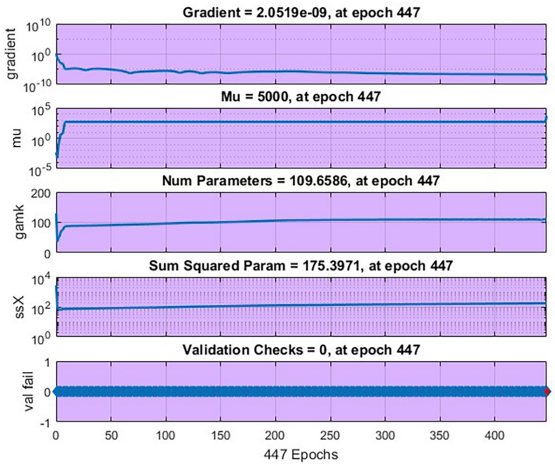

(c) Training state of S_α

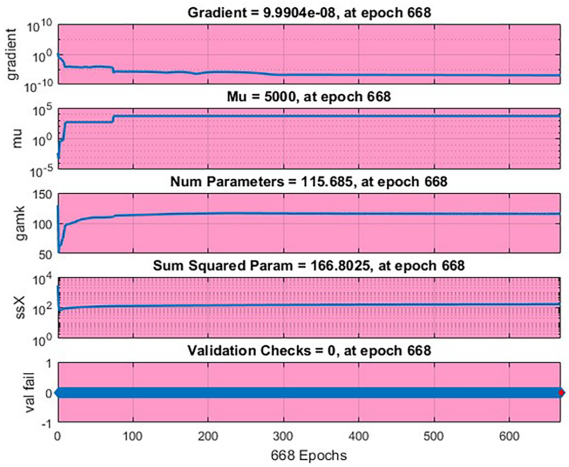

(d) Training state of M

Figure 5: (Continued)

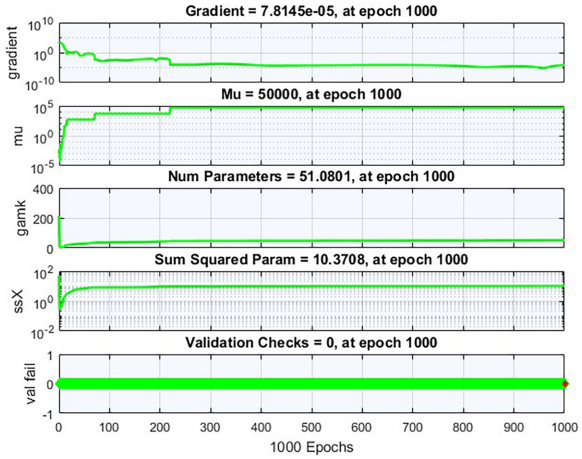

(e) Training state of T

Figure 5: Training state (case I with NARX-BRBNN).

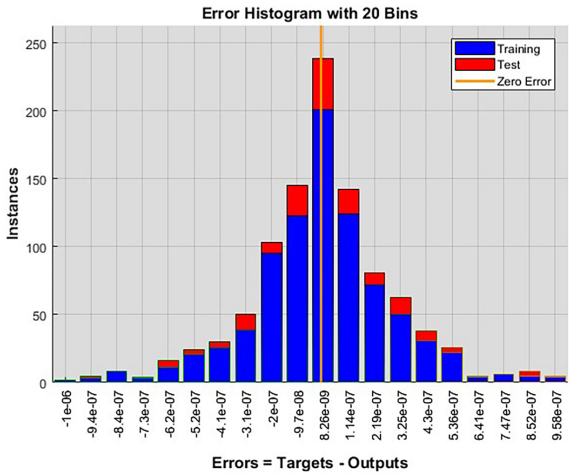

(a) Analysis of the error histogram for F

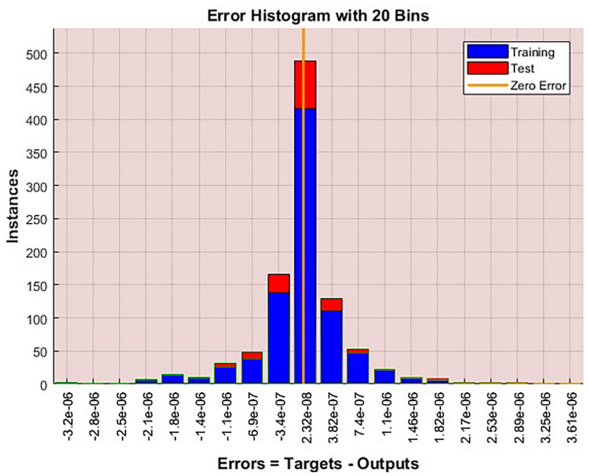

(b) Analysis of the error histogram for I

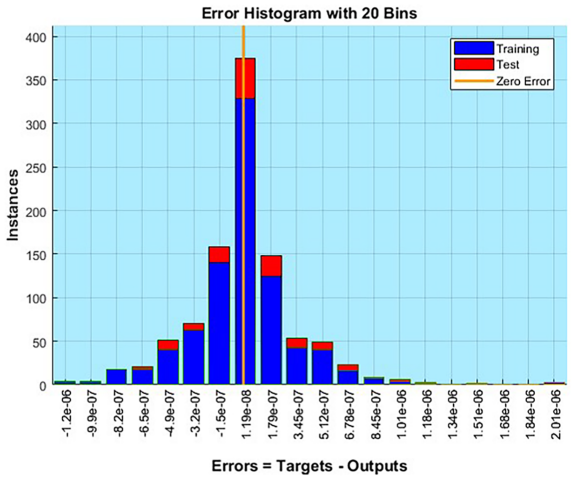

(c) Analysis of the error histogram for S_α

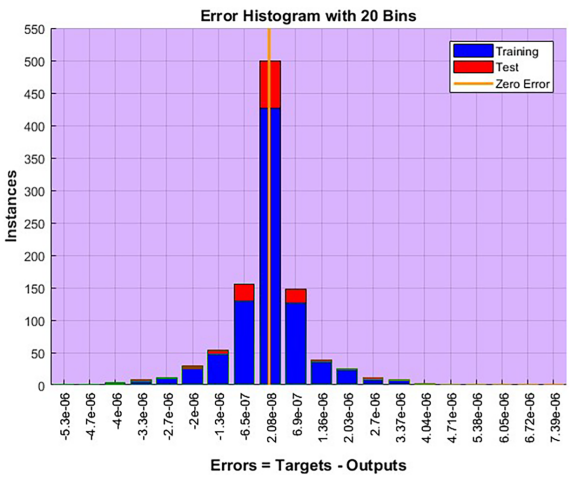

(d) Analysis of the error histogram for M

Figure 6: (Continued)

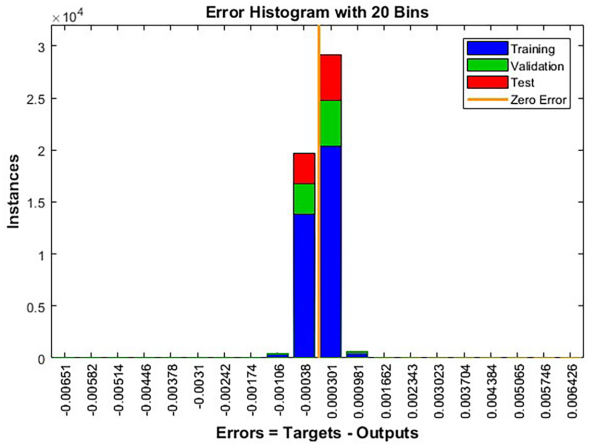

(e) Analysis of the error histogram for T

Figure 6: Error histogram (case I with NARX-BRBNN).

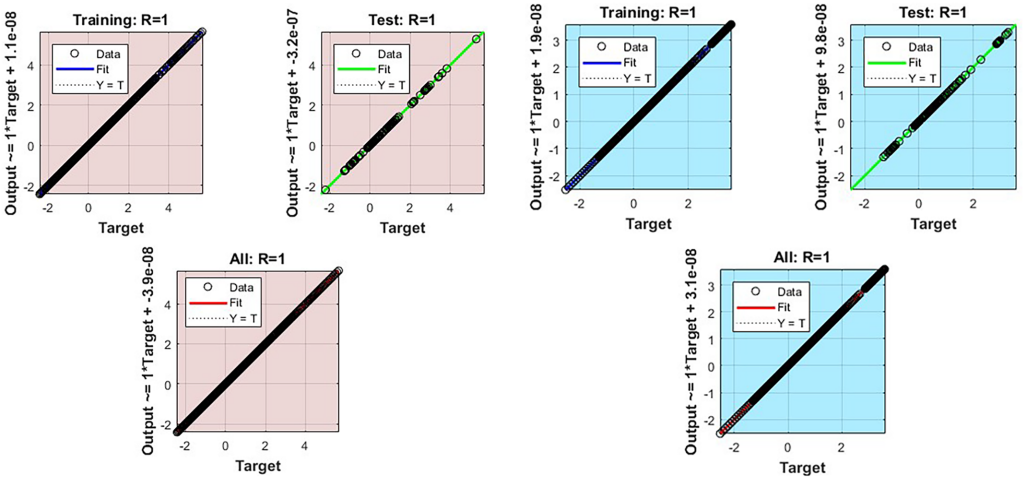

(a) Regression analysis for F

(b) Regression analysis for I

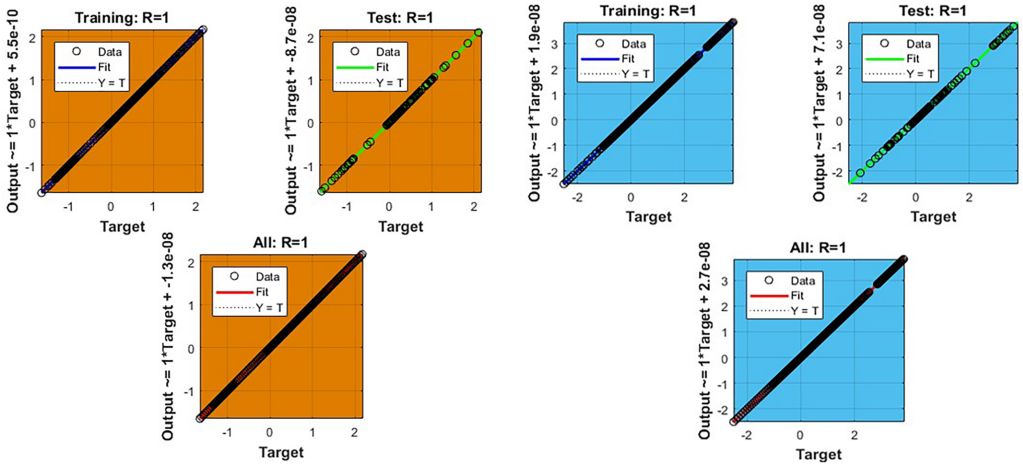

(c) Regression analysis for S_α

(d) Regression analysis for M

Figure 7: (Continued)

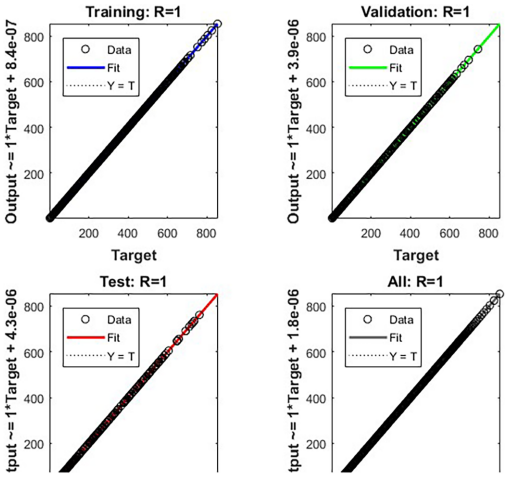

(e) Regression analysis for T

Figure 7: Regression analysis (case I with NARX-BRBNN).

Figs. 8–12 illustrate the comparison of numerical results with a predicted solution of the NARX-BRBNN scheme, and Absolute Error (AE) values for solving the FODE-BD model. The comparison between the computed and reference solutions is depicted in Figs. 8a–12a, demonstrating the effectiveness of the proposed computational framework. The accuracy and efficiency of the NARX-BRBNN approach are validated through the overlap between the obtained results and reference solutions, signifying the method's robustness in capturing the disease dynamics. The gradient is the sum of all the derivatives of the error function of each weight and bias, SSX is the Euclidean sum of all weights and biases, and Mu is the damping factor. It helps the algorithm to adapt between gradient descent and the Gauss-Newton method to update weights and biases. The AE performance of the NARX-BRBNN for solving the FODE-BD model is presented in Figs. 8b–12b. Fig. 8b displays the AE values for the density of functioning neurons $F(t)$ compartment, which range from E−07 to E−02. The AE values for the density of infected neuronal cells $I(t)$ compartment are shown in Fig. 9b, ranging between E−07 to E−02. For the extracellular α-synuclein capacity weight $S_{\alpha}(t)$ compartment as given in Fig. 10b, AE values range from E−08 to E−03. The AE values for the density of activated microglia $M(t)$ compartment are observed between E-07 to E-03 as given in Fig. 11b. Fig. 12b illustrates the AE values for the density of activated T-cells $T(t)$ compartment ranging between E−07 to E−03. These calculated AE values affirm the precision and reliability of the NARX-BRBNN methodology for solving the FODE-BD model, demonstrating its effectiveness in accurately modeling the disease transmission dynamics. Table 3 elaborates the statistical results of NARX-BRBNN which incorporates performance, gradient, mu, final epoch, etc., recorded during training.

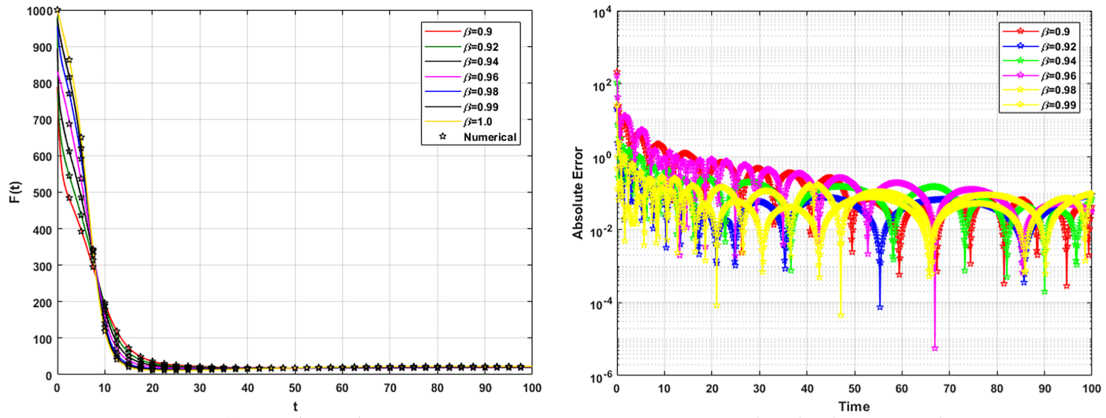

(a) Comparison plot (b) Absolute error plot

Figure 8: Deviations for $F(t)$.

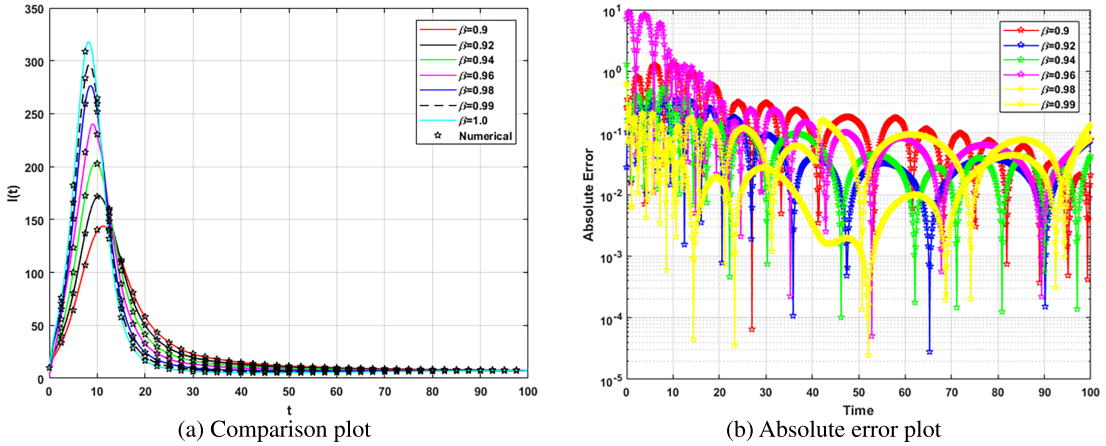

(a) Comparison plot (b) Absolute error plot

Figure 9: Deviations for $I(t)$.

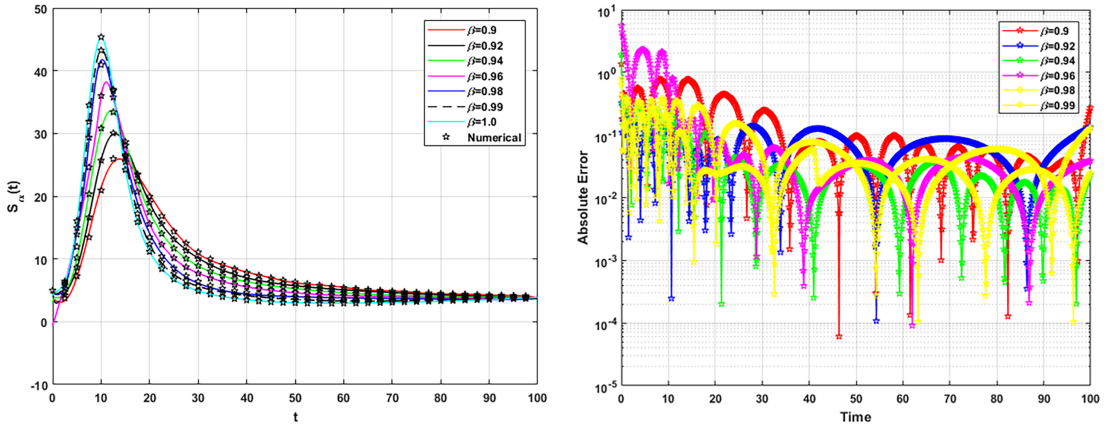

(a) Comparison plot (b) Absolute error plot

Figure 10: Deviations for $S_\alpha(t)$.

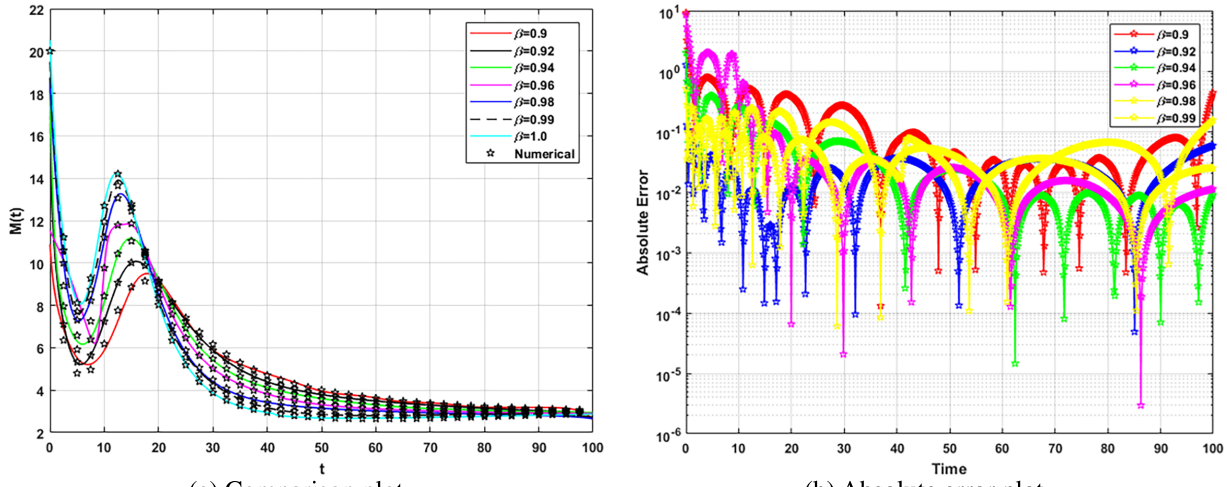

(a) Comparison plot (b) Absolute error plot

Figure 11: Deviations for $M(t)$.

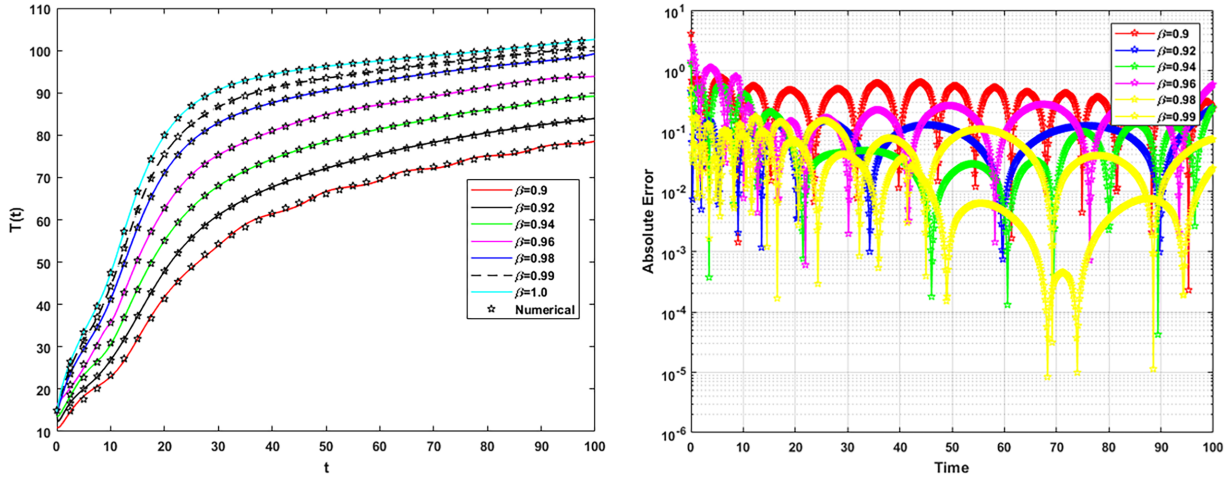

(a) Comparison plot (b) Absolute error plot

Figure 12: Deviations for $T(t)$.

6 Conclusion

The numerical performance of the fractional order differential equations based brain disease (FODE-BD) model has been analyzed in the present study by utilizing the Mittag-Leffler framework of Nonlinear Autoregressive with External Input Bayesian Regularized Backpropagated Neural Network (NARX-BRBNN). Nonlinear FODE-BD model is segregated into five classes, which correspond to functioning neurons, infected neurons, extracellular a-synuclein, microglia activation, and T-cell activation. The following are some important conclusions drawn from the study:

- Fractal fractional derivatives have been utilized to obtain accurate results for the mathematical FODE-BD model in this study.
- Seven different FODE-BD variations of fractional order (η = 0.90, 0.92, 0.94, 0.96, 0.98, 0.99, 1.0) have been solved by implementing the NARX-BRBNN approach.
- Statistical selection has been conducted for solving the FODE-BD model, with 70% allocated for training and 15% each for both testing and validation datasets (standard split).

- The accuracy of the NARX-BRBNN framework has been demonstrated by comparing the obtained solutions of NARX-BRBNN with reference solutions of the Adams method.
- Effective reference solutions have been generated using the Adams predictor-corrector method for fractional differential equations using Matlab.
- The efficiency and reliability of the stochastic NARX-BRBNN approach have been examined through simulations, with results such as time series response, regression performance, correlation analysis, and error histogram evaluations.
- From the basic reproduction number, R_0, and sensitivity analysis, it is found that the secretion rate (δ_1), infection rate (γ), neuron production (Π_N), neuron death (μ_N), and microglia deactivation (d_M).
- The advantages offered by the NARX-BRBNN surrogate model include faster computation after offline learning, ability to cope with intricate fractional dynamics without requiring continuous numerical integration, and Bayesian regularization, which helps improve generalization and prevents overfitting for different fractional values.

Further research should focus on enhancing the fractional order model by including more biological details (such as α-synuclein spatial diffusion, introducing other types of immune cells, etc.) and exploring other neural network structures, such as GM-NNs-HGA-SQP, which has shown excellent performance in recent studies. Furthermore, confirming the findings of this study using experimental/clinical data, which was not included in the current study but is an important aspect for future work. Using real-world data to estimate model parameters could significantly increase the clinical applicability of the presented methodology. Because of its flexibility, the proposed methodology allows for adaptation to various other domains of mathematical modeling, particularly in other neurodegenerative illnesses.

Acknowledgement: The authors extend their appreciation to Prince Sattam bin Abdulaziz University for funding this research work through the project number (PSAU/2025/01/38405).

Funding Statement: Prince Sattam bin Abdulaziz University (PSAU/2025/01/38405).

Author Contributions: Conceptualization: Kottakkaran Sooppy Nisar, Muhammad Farman; Formal analysis: Mohammed Altaf Ahmed, Mohammad Tabish; Investigation: Kottakkaran Sooppy Nisar, Muhammad Farman, Ali Hasan; Methodology: Kottakkaran Sooppy Nisar, Muhammad Farman; Software: Kottakkaran Sooppy Nisar, Muhammad Farman, Ali Hasan, Mohammed Altaf Ahmed, Mohammad Tabish; Validation: Kottakkaran Sooppy Nisar, Mohammed Altaf Ahmed, Mohammad Tabish; Writing—Original Draft: Kottakkaran Sooppy Nisar, Muhammad Farman, Ali Hasan, Mohammed Altaf Ahmed, Mohammad Tabish; Writing Review and Editing: Kottakkaran Sooppy Nisar, Mohammed Altaf Ahmed, Mohammad Tabish. All authors reviewed and approved the final version of the manuscript.

Availability of Data and Materials: The datasets generated and/or analysed during the current study are available from the corresponding author on reasonable request.

Ethics Approval: Not applicable.

Conflicts of Interest: The authors declare no conflicts of interest.

References

1. Zehra A, Naik PA, Hasan A, Farman M, Nisar KS, Chaudhry F, et al. Physiological and chaos effect on dynamics of neurological disorder with memory effect of fractional operator: a mathematical study. Comput Methods Programs Biomed. 2024;250(4):108190. doi:10.1016/j.cmpb.2024.108190.
2. D'Angelo E, Antonietti A, Casali S, Casellato C, Garrido JA, Luque NR, et al. Modeling the cerebellar microcircuit: new strategies for a long-standing issue. Front Cell Neurosci. 2016;10:176. doi:10.3389/fncel.2016.00176.

3. Avutu SR, Paul S, Bhatia D. Smart rehabilitation for neuro-disability: a review. In: Application of biomedical engineering in neuroscience. Singapore: Springer; 2019. p. 477–90. doi:10.1007/978-981-13-7142-4_24.
4. Chen K, Hwu T, Kashyap HJ, Krichmar JL, Stewart K, Xing J, et al. Neurorobots as a means toward neuroethology and explainable AI. Front Neurorobot. 2020;14:570308. doi:10.3389/fnbot.2020.570308.
5. D'Angelo E, Solinas S, Garrido J, Casellato C, Pedrocchi A, Mapelli J, et al. Realistic modeling of neurons and networks: towards brain simulation. Funct Neurol. 2013;28(3):153–66.
6. Lin CL, Zhu YH, Cai WH, Su YS. Recent synergies of machine learning and neurorobotics: a bibliometric and visualized analysis. Symmetry. 2022;14(11):2264. doi:10.3390/sym14112264.
7. Khonsari RH, Calvez V. The origins of concentric demyelination: self-organization in the human brain. PLoS One. 2007;2(1):e150. doi:10.1371/journal.pone.0000150.
8. Lombardo MC, Barresi R, Bilotta E, Gargano F, Pantano P, Sammartino M. Demyelination patterns in a mathematical model of multiple sclerosis. J Math Biol. 2017;75(2):373–417. doi:10.1007/s00285-016-1087-0.
9. Elettreby FM, Ahmed E. A simple mathematical model for relapsing-remitting multiple sclerosis (RRMS). Med Hypotheses. 2020;135(4):109478. doi:10.1016/j.mehy.2019.109478.
10. Shah K, Alqudah MA, Jarad F, Abdeljawad T. Semi-analytical study of Pine Wilt disease model with convex rate under Caputo-Febrizio fractional order derivative. Chaos Solit. 2020;135(2):109754. doi:10.1016/j.chaos.2020.109754.
11. Shah K, Abdeljawad T. Study of a mathematical model of COVID-19 outbreak using some advanced analysis. Waves Random Complex Media. 2026;36(1):1–8. doi:10.1080/17455030.2022.2149890.
12. Podlubny I. Fractional-order systems and PI/sup /spl lambda//D/sup /spl mu//-controllers. IEEE Trans Autom Control. 1999;44(1):208–14. doi:10.1109/9.739144.
13. Atangana A, Baleanu D, Alsaedi A. Analysis of time-fractional Hunter-Saxton equation: a model of neumatic liquid crystal. Open Phys. 2016;14(1):145–9. doi:10.1515/phys-2016-0010.
14. Khan A, Ali A, Ahmad S, Saifullah S, Nonlaopon K, Akgül A. Nonlinear Schrdinger equation under non-singular fractional operators: a computational study. Results Phys. 2022;43:106062. doi:10.1016/j.rinp.2022.106062.
15. Nisar KS, Ciancio A, Ali KK, Osman MS, Cattani C, Baleanu D, et al. On beta-time fractional biological population model with abundant solitary wave structures. Alex Eng J. 2022;61(3):1996–2008. doi:10.1016/j.aej.2021.06.106.
16. Arqub OA, Al-Smadi M, Almusawa H, Baleanu D, Hayat T, Alhodaly M, et al. A novel analytical algorithm for generalized fifth-order time-fractional nonlinear evolution equations with conformable time derivative arising in shallow water waves. Alex Eng J. 2022;61(7):5753–69. doi:10.1016/j.aej.2021.12.044.
17. Cuahutenango-Barro B, Taneco-Hernández MA, Lv YP, Gómez-Aguilar JF, Osman MS, Jahanshahi H, et al. Analytical solutions of fractional wave equation with memory effect using the fractional derivative with exponential kernel. Results Phys. 2021;25:104148. doi:10.1016/j.rinp.2021.104148.
18. Rashid S, Kubra KT, Sultana S, Agarwal P, Osman MS. An approximate analytical view of physical and biological models in the setting of Caputo operator via Elzaki transform decomposition method. J Comput Appl Math. 2022;413:114378. doi:10.1016/j.cam.2022.114378.
19. Ak T, Osman MS, Kara AH. Polynomial and rational wave solutions of Kudryashov-Sinelshchikov equation and numerical simulations for its dynamic motions. J Appl Anal Comput. 2020;10(5):2145–62. doi:10.11948/20190341.
20. Xu C, Farman M, Hasan A, Akgül A, Zakarya M, Albalawi W, et al. Lyapunov stability and wave analysis of COVID-19 omicron variant of real data with fractional operator. Alex Eng J. 2022;61(12):11787–802. doi:10.1016/j.aej.2022.05.025.
21. Nisar KS, Farman M. A review on fuzzy fractional order modeling in health systems with application to cardiovascular disease. Int J Math Comput Eng. 2026. doi:10.2478/ijmce-2026-0014.
22. Cieza Altamirano G. A stochastic neural network process for the fractional order lungs cancer operation system. Int J Math Comput Eng. 2026. doi:10.2478/ijmce-2026-0011.
23. Gergley M, Chellamuthu V. A mathematical model of HPA axis dynamics and impacts of alcohol consumption. Int J Math Comput Eng. 2026. doi:10.2478/ijmce-2026-0006.

24. Devi AS, Naik PA, Boulaaras S, Sene N, Huang Z. Understanding the transmission mechanism of HIV/TB co-infection using fractional framework with optimal control. Int J Numer Model Electron Netw Devices Fields. 2025;38(4):e70097. doi:10.1002/jnm.70097.
25. Naik PA, Yavuz M, Qureshi S, Owolabi KM, Soomro A, Ganie AH. Memory impacts in hepatitis C: a global analysis of a fractional-order model with an effective treatment. Comput Methods Programs Biomed. 2024;254(1):108306. doi:10.1016/j.cmpb.2024.108306.
26. Amilo D, Sadri K, Hincal E, Hafez M. A hybrid computational framework for Parkinson's disease prediction using fractional-order modeling and machine learning via vocal biomarkers. Ain Shams Eng J. 2026;17(1):103889. doi:10.1016/j.asej.2025.103889.
27. Khirsariya SR, Noori N. Fractal-fractional modeling of chronic myelogenous leukemia immune dynamics using Laguerre wavelets method. Sci Rep. 2026;16(1):860. doi:10.1038/s41598-026-43767-3.
28. Samreen A, Baleanu D, Messaoudi S, Boulaaras S, Akram S, ur Rahman M. Modeling the dynamics of malaria with infected immigrants using fractal-fractional techniques with deep neural networks. Asian J Control. 2026;28(1):182–99. doi:10.1002/asjc.3641.
29. Yurtoglu M, Yapiskan D, Bonyah E, Iskender Eroglu BB, Avci D, Torres DF. Dynamic analysis and optimal prevention strategies for monkeypox spread modeled via the mittag-leffler kernel. Fractal Fract. 2026;10(1):44. doi:10.3390/fractalfract10010044.
30. Madani N, Hammouch Z, Jafari H. Fractal-fractional modeling of drug addiction dynamics: capturing memory-driven effects. Math Methods Appl Sci. 2026;49(3):2114–28. doi:10.1002/mma.70232.
31. Talib A, Farman M, Ibrahim AU, Nisar KS, Sambas A. Dynamics predictive of neurodegenerative diseases by using the generalized Caputo operator through computational and multiscale modeling. J Appl Math Comput. 2025;71(5):6289–320. doi:10.1007/s12190-025-02526-9.
32. Hao W, Lenhart S, Petrella JR. Optimal anti-amyloid-beta therapy for Alzheimer's disease via a personalized mathematical model. PLoS Comput Biol. 2022;18(9):e1010481. doi:10.1371/journal.pcbi.1010481.
33. Alkahtani BST, Alzaid SS. Stochastic fractional model of Alzheimer's disease. Results Phys. 2021;23(1):103977. doi:10.1016/j.rinp.2021.103977.
34. Atangana A, Baleanu D. New fractional derivatives with nonlocal and non-singular kernel: theory and application to heat transfer model. Therm Sci. 2016;2(3):763–9. doi:10.2298/TSCI160111018A.
35. Diekmann O, Heesterbeek JA, Roberts MG. The construction of next-generation matrices for compartmental epidemic models. J R Soc Interface. 2010;7(47):873–85. doi:10.1098/rsif.2009.0386.
36. Al-Refai M, Luchko Y. Comparison principles for solutions to the fractional differential inequalities with the general fractional derivatives and their applications. J Differ Equ. 2022;319(2):312–24. doi:10.1016/j.jde.2022.02.054.
37. Kilbas AA, Srivastava HM, Trujillo JJ. Theory and applications of fractional differential equations. In: North-holland mathematics studies. Amsterdam, The Netherlands: Elsevier Science; 2006.
38. Kahoui MH, Otto A. Stability of disease free equilibria in epidemiological models. Math Comput Sci. 2009;2(3):517–33. doi:10.1007/s11786-008-0068-0.
39. Atangana A. Fractal-fractional differentiation and integration: connecting fractal calculus and fractional calculus to predict complex system. Chaos Solit. 2017;102(5):396–406. doi:10.1016/j.chaos.2017.04.027.
40. Vargas-De-León C. Volterra-type Lyapunov functions for fractional-order epidemic systems. Commun Nonlinear Sci Numer Simul. 2015;24(1–3):75–85. doi:10.1016/j.cnsns.2014.12.013.